

Runge-Kutta Discontinuous Galerkin Method for the Boltzmann Equation

by

Ho Man Lui

Submitted to the School of Engineering
in partial fulfillment of the requirements for the degree of
Master of Science in Computation for Design and Optimization
at the

MASSACHUSETTS INSTITUTE OF TECHNOLOGY

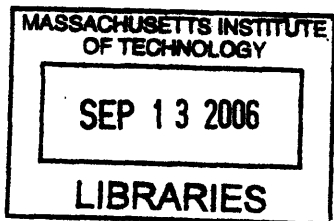
September 2006

© Massachusetts Institute of Technology 2006. All rights reserved.

Author
School of Engineering
Aug 11, 2006

Certified by
Nicolas G. Hadjiconstantinou
Associate Professor
Thesis Supervisor

Accepted by
Jaime Peraire
Professor of Aeronautics and Astronautics
Codirector, Computation for Design and Optimization



ARCHIVES

Runge-Kutta Discontinuous Galerkin Method for the Boltzmann Equation

by

Ho Man Lui

Submitted to the School of Engineering
on Aug 11, 2006, in partial fulfillment of the
requirements for the degree of
Master of Science in Computation for Design and Optimization

Abstract

In this thesis we investigate the ability of the Runge-Kutta Discontinuous Galerkin (RKDG) method to provide accurate and efficient solutions of the Boltzmann equation. Solutions of the Boltzmann equation are desirable in connection to small scale science and technology because when characteristic flow length scales become of the order of, or smaller than, the molecular mean free path, the Navier-Stokes description fails. The prevalent Boltzmann solution method is a stochastic particle simulation scheme known as Direct Simulation Monte Carlo (DSMC). Unfortunately, DSMC is not very effective in low speed flows (typical of small scale devices of interest) because of the high statistical uncertainty associated with the statistical sampling of macroscopic quantities employed by this method.

This work complements the recent development of an efficient low noise method for calculating the collision integral of the Boltzmann equation, by providing a high-order discretization method for the advection operator balancing the collision integral in the Boltzmann equation. One of the most attractive features of the RKDG method is its ability to combine high-order accuracy, both in physical space and time, with the ability to capture discontinuous solutions. The validity of this claim is thoroughly investigated in this thesis. It is shown that, for a model collisionless Boltzmann equation, high-order accuracy can be achieved for continuous solutions; whereas for discontinuous solutions, the RKDG method, with or without the application of a slope limiter such as a viscosity limiter, displays high-order accuracy away from the vicinity of the discontinuity.

Given these results, we developed a RKDG solution method for the Boltzmann equation by formulating the collision integral as a source term in the advection equation. Solutions of the Boltzmann equation, in the form of mean velocity and shear stress, are obtained for a number of characteristic flow length scales and compared to DSMC solutions. With a small number of elements and a low order of approximation in physical space, the RKDG method achieves similar results to the DSMC method. When the characteristic flow length scale is small compared to the mean free path (i.e. when the effect of collisions is small), oscillations are present in the

mean velocity and shear stress profiles when a coarse velocity space discretization is used. With a finer velocity space discretization, the oscillations are reduced, but the method becomes approximately five times more computationally expensive. We show that these oscillations (due to the presence of propagating discontinuities in the distribution function) can be removed using a viscosity limiter at significantly smaller computational cost.

Thesis Supervisor: Nicolas G. Hadjiconstantinou

Title: Associate Professor

Acknowledgments

The research experience has been an enriching and fulfilling one.

My sincere appreciation goes to my supervisor Prof. Nicolas G. Hadjiconstantinou for his guidance and advice on the project.

I am also very thankful towards Lowell, who has helped me with the collision integral, DSMC code and in many aspects of my research.

Without the help of Husain in getting me an account on the computer cluster, I would not have been able to generate the results for this work.

I would like to express my gratitude to Thomas for giving me many useful tips in using DSMC and LaTeX.

Thanks to my fellow research students Lowell, Thomas, Ghassan and Husain in 3-355A, the lab is such a lively place.

Special thanks go to Vinh Tan Nguyen of the Singapore-MIT Alliance who advised me a great deal with his experience in the RKDG method. He has also given me precious ideas in the area of slope limiting.

My deepest gratitude goes to my family for their endless support and belief in me.

Last but not least, I would like to thank the Singapore-MIT Alliance for sponsoring this project.

THIS PAGE INTENTIONALLY LEFT BLANK

Contents

1	Introduction	15
1.1	Motivation	15
1.2	Kinetic description and the Boltzmann equation	16
1.3	Direct numerical method for the Boltzmann equation	16
1.4	Thesis outline	17
2	Background	19
2.1	Nondimensional Boltzmann equation	19
2.2	Couette flow problem	20
2.3	Hydrodynamic fields	21
2.4	Collisionless Boltzmann equation	22
3	Runge-Kutta discontinuous Galerkin method (RKDG)	23
3.1	Discontinuous Galerkin discretization	24
3.1.1	Physical space elements	24
3.1.2	Modal basis	25
3.1.3	Initialization of distribution function	27
3.1.4	Discretized collisionless Boltzmann equation	27
3.2	Runge-Kutta time discretization	31
3.3	Slope limiter	33
3.3.1	Generalized moment limiter	34
3.3.2	Viscosity limiter	36
3.4	Implementation	37

3.5	Error measurement	38
4	A test problem with continuous solutions	39
4.1	The test problem	39
4.2	Discontinuous Galerkin discretization	40
4.3	Runge-Kutta time discretization	41
4.3.1	Left “wall” element	42
4.4	Implementation	43
4.5	Error convergence	44
4.5.1	Arbitrary precision calculations	45
5	A test problem with discontinuous solutions	51
5.1	The test problem	51
5.2	Discontinuous Galerkin discretization	52
5.3	Runge-Kutta time discretization schemes	53
5.4	Slope limiter	53
5.5	Implementation	54
5.6	Error convergence	55
5.6.1	Arbitrary precision calculations	56
6	Runge-Kutta discontinuous Galerkin method for the Boltzmann equation	65
6.1	Discretization of velocity space	65
6.2	Discontinuous Galerkin discretization	66
6.3	Collision integral	67
6.4	Runge-Kutta time discretization	67
6.5	Slope limiter	69
6.6	Implementation	69
6.7	Comparison with direct simulation Monte Carlo (DSMC)	70
6.7.1	Viscosity limiter	72

7 Conclusion	79
7.1 Future work	80
7.1.1 High-order physical space discretization	80
7.1.2 Viscosity in the viscosity limiter	80
7.1.3 High-order velocity space discretization	80
A Gaussian quadrature	83

THIS PAGE INTENTIONALLY LEFT BLANK

List of Figures

4-1	$\ \varepsilon\ $ against Δz for $\Delta t = 10^{-4}$ using RK3ssp	47
4-2	$\ \varepsilon\ $ against Δz for $\Delta t = 10^{-4}$ using RK4std	47
4-3	$\ \varepsilon\ _1$ against Δt for $p = 5$, with Arprec 100 precision digits	47
5-1	Numerical solutions for $\Delta t = 10^{-4}$, $n = 10$ and $p = 5$ with no limiter, moment limiter, generalized moment limiter and viscosity limiter using RK3ssp	58
5-2	$\ \varepsilon\ _1$ against Δz for $\Delta t = 10^{-4}$ with no limiter, moment limiter, generalized moment limiter and viscosity limiter using RK3ssp	59
5-3	$\ \varepsilon\ _1$ against Δt for $p = 5$ with no limiter, generalized slope limiter and viscosity limiter using RK3ssp, with Arprec 100 precision digits	60
6-1	Mean velocity and shear stress in Couette flow for $\text{Kn} = 0.1$ and $u_{\text{wall}} = \pm 0.1$ at $t = 0, 2.04, 4.96, 11.96$ and 30.02 . Comparison of RKDG with $n = 10$ and $p = 2$ against DSMC	74
6-2	Mean velocity and shear stress in Couette flow for $\text{Kn} = 1$ and $u_{\text{wall}} = \pm 0.1$ at $t = 0, 0.204, 0.496, 1.016$ and 4.016 . Comparison of RKDG with $n = 10$ and $p = 2$ against DSMC	75
6-3	Mean velocity and shear stress in Couette flow for $\text{Kn} = 10$ and $u_{\text{wall}} = \pm 0.1$ at $t = 0, 0.0204, 0.0496, 0.1602$ and 0.5640 . Comparison of RKDG with $n = 10$ and $p = 2$ against DSMC	76
6-4	Mean velocity and shear stress in Couette flow for $\text{Kn} = 1$ and 10 and $u_{\text{wall}} = \pm 0.1$. Comparison of RKDG with $n = 10$, $p = 2$ and viscosity limiter against DSMC	77

THIS PAGE INTENTIONALLY LEFT BLANK

List of Tables

3.1	CFL numbers for RK3ssp for polynomials of order p	32
4.1	Convergence with respect to Δz for $\Delta t = 10^{-4}$ using RK3ssp	48
4.2	Convergence with respect to Δz for $\Delta t = 10^{-4}$ using RK4std	49
4.3	Convergence with respect to Δt for $p = 5$, with Arprec 100 precision digits	49
5.1	Convergence with respect to Δz for $\Delta t = 10^{-4}$ with no limiter and moment limiter using RK3ssp	61
5.2	Convergence with respect to Δz for $\Delta t = 10^{-4}$ with generalized moment limiter and viscosity limiter using RK3ssp	62
5.3	Convergence with respect to Δt for $p = 5$ with no slope limiter, generalized moment limiter and viscosity limiter using RK3ssp, with Arprec 100 precision digits	63
6.1	Test parameters for $\text{Kn} = 0.1, 1$ and 10	73
6.2	Test parameters for $\text{Kn} = 1$ and 10 with viscosity limiter	73
A.1	Gauss points and weights for $n_g \leq 7$	84

THIS PAGE INTENTIONALLY LEFT BLANK

Chapter 1

Introduction

1.1 Motivation

In dilute gas flows the breakdown of the Navier-Stokes description can be quantified by the Knudsen number, Kn , defined here as the ratio between the molecular mean free path λ and the characteristic flow length scale [20]. It is generally accepted that the Navier-Stokes description fails for $\text{Kn} \gtrsim 0.1$. Flows characterized by $\text{Kn} \gtrsim 0.1$ are usually modeled using a kinetic description and the Boltzmann equation (see section 1.2).

The prevalent solution method for the Boltzmann equation is a stochastic particle simulation method known as direct simulation Monte Carlo (DSMC). Although generally very efficient, DSMC suffers from a serious disadvantage when used to simulate low speed flows which are of interest currently. The statistical sampling employed by DSMC for obtaining macroscopic fields from microscopic data has a slow convergence rate which makes the cost of simulation of low-signal (low-speed) flows prohibitive. In this thesis we evaluate an alternative solution method.

1.2 Kinetic description and the Boltzmann equation

Within kinetic theory, a dilute gas can be described using the single-particle distribution function $f(\vec{r}, \vec{v}, t)$ which is proportional to the probability of a gas particle being found at (\vec{r}, \vec{v}) at time t . Here, $\vec{r} = (x, y, z)$ is the physical position vector, while $\vec{v} = (v_x, v_y, v_z)$ is the velocity space vector. The evolution of the distribution function is governed by the Boltzmann equation which, in the absence of external forces, is given by [20, 1] as

$$\frac{\partial f}{\partial t} + \vec{v} \cdot \frac{\partial f}{\partial \vec{r}} = \left[\frac{\partial f}{\partial t} \right]_{\text{coll}} \quad (1.1)$$

where $\left[\frac{\partial f}{\partial t} \right]_{\text{coll}}$ denotes the effect of collisions given by a collision integral. The derivation of the above Boltzmann equation can be found in [6, 18, 20] and shall not be discussed here. In the interest of simplicity, the full form of the collision integral will not be given here since it will be treated as a precalculated source term in our numerical implementation.

1.3 Direct numerical method for the Boltzmann equation

To address the deficiency associated with DSMC, a particle-like method has been developed to evaluate the collision integral in [4] as part of a direct numerical method for solving the Boltzmann equation. This approach has been shown to be both efficient and accurate compared to DSMC. However, so far little attention has been paid to the discretization of the advection operator within this formulation. In particular, in [4] the physical space was discretized with the finite volume method and time was discretized using a simple splitting scheme. The objective of this thesis is to evaluate an alternative discretization approach which seems very well suited to the physics of the Boltzmann equation.

The Runge-Kutta discontinuous Galerkin (RKDG) method [10] provides a very

promising approach for discretizing the advection operator. RKDG is a high-order method in both physical space and time discretization, and it is effective even in the presence of discontinuities. In this thesis, we develop and extensively test an algorithm which adapts the discontinuous Galerkin physical space discretization and Runge-Kutta time discretization from the RKDG method, and combines it with the efficient collision integral evaluation method of [4] to formulate a direct numerical scheme to solve the Boltzmann equation. As we will show, this direct numerical algorithm is an efficient and accurate method; in particular it is significantly more effective than DSMC for low-speed flows.

1.4 Thesis outline

In the next chapter we give some background information on the nondimensional form of the Boltzmann equation, the Couette flow problem, the hydrodynamic fields from the moments of the distribution function, and the collisionless Boltzmann equation. The RKDG method is described in chapter 3 from the perspective of solving the collisionless Boltzmann equation. Chapter 4 demonstrates the application of the RKDG method to a test problem which admits continuous solutions. This verifies the high-order accuracy of the RKDG method both in physical space and time. In chapter 5, the RKDG method is applied to a problem in which the initial data and boundary conditions give rise to an analytical solution that has a discontinuity propagating in the physical space over time. Successfully applying RKDG on this test problem shall show that RKDG is effective in solving a discontinuous problem. Finally in chapter 6, the Boltzmann equation with the collision integral is solved. The approach used here is to treat the collision integral as a source term. The distribution function advances in time with a strong stability-preserving Runge-Kutta time discretization scheme. Conclusions drawn from this thesis and recommendations for future research in this topic are given in chapter 7.

THIS PAGE INTENTIONALLY LEFT BLANK

Chapter 2

Background

2.1 Nondimensional Boltzmann equation

In this thesis we use the same nondimensional form of the Boltzmann equation as in [3].

The nondimensional units, denoted by a superscript *, are defined by the following relationships

$$t = \bar{t}t^* \quad (2.1)$$

$$\vec{r} = \lambda\vec{r}^* \quad (2.2)$$

$$\vec{v} = \bar{v}\vec{v}^* \quad (2.3)$$

$$f = \frac{\bar{n}}{\bar{v}^3}f^* \quad (2.4)$$

where \bar{n} is a characteristic number density, k is the Boltzmann constant, \bar{T} is a characteristic temperature, \bar{d} is a characteristic molecular diameter, m is the molecular mass,

$$\bar{v} = \sqrt{\frac{2k\bar{T}}{m}} \quad (2.5)$$

is the most probable thermal speed,

$$\lambda = \frac{1}{\sqrt{2}\pi\bar{d}^2\bar{n}} \quad (2.6)$$

is the molecular mean free path, and

$$\bar{t} = \frac{\sqrt{\pi} \lambda}{2 \bar{v}} \quad (2.7)$$

is the collision time.

The nondimensional form of the Boltzmann equation

$$\frac{\partial f^*}{\partial t^*} + \frac{\sqrt{\pi}}{2} \vec{v}^* \cdot \frac{\partial f^*}{\partial \vec{r}^*} = \frac{\sqrt{\pi}}{2} \left[\frac{\partial f^*}{\partial t^*} \right]_{\text{coll}} \quad (2.8)$$

can be derived by substituting the nondimensional units into equation (1.1).

Since only the nondimensional form of the Boltzmann equation is to be solved in this work, the superscript $*$ is omitted in the rest of the thesis. We shall also omit the constant $\frac{\sqrt{\pi}}{2}$ multiplying the collision integral in the interest of simplicity. This omission is not to be interpreted as affecting the collision rate, but rather $\left[\frac{df}{dt} \right]_{\text{coll}}$ being a shorthand for $\frac{\sqrt{\pi}}{2} \left[\frac{\partial f}{\partial t} \right]_{\text{coll}}$. In summary, the nondimensional Boltzmann equation solved in this thesis is given by

$$\frac{\partial f}{\partial t} + \frac{\sqrt{\pi}}{2} \vec{v} \cdot \frac{\partial f}{\partial \vec{r}} = \left[\frac{df}{dt} \right]_{\text{coll}} \quad (2.9)$$

2.2 Couette flow problem

Couette flow refers to the flow between two parallel infinitely large walls in the xy plane, separated by a dimensionless distance L in the z direction, and moving relative to one another in the x direction. This flow will serve here as one of the main test problems of our RKDG solution method because it combines the simplicity of a one-dimensional problem (gradients in x and y directions are zero) while retaining all the essential physics of interest. Note in particular that the transient evaluation of this flow from a rest state to steady state involves the propagation of discontinuities in the distribution function across the physical space z , making this problem a very stringent test of the RKDG method. The nondimensional Boltzmann equation for

this one-dimensional problem reads

$$\frac{\partial f}{\partial t} + \frac{\sqrt{\pi}}{2} v_z \frac{\partial f}{\partial z} = \left[\frac{df}{dt} \right]_{\text{coll}} \quad (2.10)$$

The Knudsen number is given by $\text{Kn} = \frac{1}{L}$. The left wall is moving at $u_{x\text{lw}} = -0.1$, and the right wall is moving at $u_{x\text{rw}} = 0.1$. The associated boundary condition for distribution function is

$$\begin{aligned} f_{\text{lw}} &= \bar{n} \exp \left(-\frac{(v_x - u_{x\text{lw}})^2 + v_y^2 + v_z^2}{\bar{v}^2} \right) \quad \text{if } v_z \geq 0 \\ f_{\text{rw}} &= \bar{n} \exp \left(-\frac{(v_x - u_{x\text{rw}})^2 + v_y^2 + v_z^2}{\bar{v}^2} \right) \quad \text{if } v_z < 0 \end{aligned} \quad (2.11)$$

where f_{lw} and f_{rw} are the boundary conditions of the distribution function at left and right walls respectively.

The distribution function in the gas at $t = 0$ is the equilibrium Maxwell-Boltzmann

$$f = \bar{n} \exp \left(-\frac{v_x^2 + v_y^2 + v_z^2}{\bar{v}^2} \right) \quad (2.12)$$

In chapter 6, we shall present the numerical solutions of the Couette flow problem using the RKDG method. The RKDG results, in the form of mean velocity and shear stress described in the next section, shall be compared to DSMC solutions.

2.3 Hydrodynamic fields

In order to assess the RKDG method against the more prevalent DSMC method, we compare the hydrodynamic fields like the mean velocity and shear stress obtained from the moments of the distribution functions evaluated by RKDG. The nondimensional mean velocity for the one-dimensional Couette flow problem is

$$\begin{aligned} u_x(z, t) &= \frac{\int v_x f(z, \vec{v}, t) d^3 \vec{v}}{\int f(z, \vec{v}, t) d^3 \vec{v}} \\ u_y(z, t) &= \frac{\int v_y f(z, \vec{v}, t) d^3 \vec{v}}{\int f(z, \vec{v}, t) d^3 \vec{v}} = 0 \end{aligned}$$

$$u_z(z, t) = \frac{\int v_z f(z, \vec{v}, t) d^3 \vec{v}}{\int f(z, \vec{v}, t) d^3 \vec{v}} = 0 \quad (2.13)$$

The nondimensional p_{xz} component of the shear stress is given by

$$\begin{aligned} p_{xz}(z, t) &= \int (v_x - u_x(z, t)) (v_z - u_z(z, t)) f(z, \vec{v}, t) d^3 \vec{v} \\ &= \int v_z (v_x - u_x(z, t)) f(z, \vec{v}, t) d^3 \vec{v} \end{aligned} \quad (2.14)$$

2.4 Collisionless Boltzmann equation

One particularly interesting limit of the Boltzmann equation is obtained when $\text{Kn} \rightarrow \infty$, in which the contribution of the collision integral goes to zero, leading to the collisionless Boltzmann equation given below

$$\frac{\partial f}{\partial t} + \frac{\sqrt{\pi}}{2} v_z \frac{\partial f}{\partial z} = 0 \quad (2.15)$$

This equation will be the focus of our investigation in chapters 4 and 5, where the convergence of the RKDG method is investigated for continuous and discontinuous solution fields respectively. The collisionless approximation allows one to reduce the considerable computational cost associated with evaluating the collision integral while retaining (and, in fact, enhancing ¹) the presence of propagating discontinuities that are central to our investigation.

¹The collision integral is generally seen to have a smoothing effect on f .

Chapter 3

Runge-Kutta discontinuous Galerkin method (RKDG)

The Runge-Kutta discontinuous Galerkin method (RKDG) is a numerical method very suitable for convection-dominated problems like the advection operator of the Boltzmann equation, a first-order hyperbolic system in which discontinuities can arise. The RKDG method has high-order accuracy in both physical space and time. The discontinuous Galerkin physical space discretization of RKDG allows high-order approximation even in the presence of discontinuities in the physical space. For time discretization, Runge-Kutta integration schemes, some of which have been specially developed for the RKDG method, ensure both stability and high-order accuracy in time.

When a discontinuous problem is involved in the hyperbolic system, oscillations can appear around the discontinuities. These oscillations can cause stability problems to the RKDG method and slope limiters need to be applied to rectify this. In section 3.3, more about slope limiters for the RKDG method shall be discussed.

In this chapter, to illustrate the RKDG method and the usage of slope limiters, the Couette flow problem is investigated for a single velocity node of $\vec{v} = (0, 0, v_z)$. The distribution function is governed by the nondimensional collisionless Boltzmann

equation

$$\frac{\partial f}{\partial t} + \frac{\sqrt{\pi}}{2} v_z \frac{\partial f}{\partial z} = 0 \quad (3.1)$$

3.1 Discontinuous Galerkin discretization

In this section we describe the discretization of the nondimensional collisionless Boltzmann equation using the discontinuous Galerkin method. The addition of collisions will be described in chapter 6.

3.1.1 Physical space elements

The physical space z is uniformly discretized into n elements of $I_j \in (z_{j-\frac{1}{2}}, z_{j+\frac{1}{2}})$, $j = 1, 2, \dots, n$. Each element has length $\Delta z = z_{j+\frac{1}{2}} - z_{j-\frac{1}{2}}$ and has its mid-point at z_j . Every element is mapped onto a reference element, which has $\xi = -1$ as the left boundary, and $\xi = 1$ as the right boundary, using the following linear transformation

$$\begin{aligned} \xi &= \frac{2}{\Delta z}(z - z_j) \\ z &= z_j + \xi \frac{\Delta z}{2} \end{aligned} \quad (3.2)$$

The derivatives of the linear transformation can be calculated

$$\begin{aligned} \frac{d\xi}{dz} &= \frac{2}{\Delta z} \\ \frac{dz}{d\xi} &= \frac{\Delta z}{2} \end{aligned} \quad (3.3)$$

A distribution function that is restricted at discrete points is denoted by a subscript h . The discrete distribution function f_h in each element I_j can be mapped onto a reference element

$$f_h(z) = f_{hj}(\xi) \quad (3.4)$$

where z and ξ are related by equation (3.2).

The advantage of mapping to the reference element is that many useful numerical

tools like Gaussian quadrature and Legendre polynomials are defined for the reference element of $\xi \in [-1, 1]$.

3.1.2 Modal basis

Each element I_j has a local space $F(I_j)$ of polynomials, which can be mapped onto a local space $\tilde{F}(\xi)$ of a reference element with the linear transformation in the previous section. In a reverse manner, $\tilde{F}(\xi)$ can also be mapped onto $F(I_j)$. The local space of the reference element is formed by modal basis functions.

The modal basis functions used in the reference element are Legendre polynomials $\psi \in \tilde{F}(\xi)$. Using Legendre polynomials of order 0 to p approximates the distribution function in the physical dimension z to the order of p [13]. The following are the Legendre polynomials of order up to $p = 6$ for the reference element of $\xi \in [-1, 1]$

$$\begin{aligned}
\psi^0(\xi) &= 1 \\
\psi^1(\xi) &= \xi \\
\psi^2(\xi) &= \frac{1}{2}(3\xi^2 - 1) \\
\psi^3(\xi) &= \frac{1}{2}(5\xi^3 - 3\xi) \\
\psi^4(\xi) &= \frac{1}{8}(35\xi^4 - 30\xi^2 + 3) \\
\psi^5(\xi) &= \frac{1}{8}(63\xi^5 - 70\xi^3 + 15\xi) \\
\psi^6(\xi) &= \frac{1}{16}(231\xi^6 - 315\xi^4 + 105\xi^2 - 5)
\end{aligned} \tag{3.5}$$

Note that the Legendre polynomials always take the following values at the boundaries

$$\begin{aligned}
\psi^k(-1) &= (-1)^k \\
\psi^k(1) &= 1
\end{aligned} \tag{3.6}$$

The Legendre polynomials have the orthogonality property [13]

$$\int_{-1}^1 \psi^i \psi^j d\xi = \frac{2}{2i+1} \delta_{ij} \quad (3.7)$$

where δ_{ij} is a delta function such that

$$\delta_{ij} = \begin{cases} 1, & i = j \\ 0, & \text{otherwise} \end{cases}$$

Due to the orthogonality of the Legendre polynomials, the following summation of integrals, where α^k is a constant corresponding to ψ^k , can also be derived for each order $l \leq p$

$$\sum_{k=0}^p \int_{-1}^1 \alpha^k \psi^k(\xi) \frac{d\psi^l}{d\xi} d\xi = \sum_m 2\alpha^m \quad (3.8)$$

$$\text{where } m = \begin{cases} l-1, l-3, \dots, 1 & \text{if } l \text{ is even} \\ l-1, l-3, \dots, 0 & \text{if } l \text{ is odd} \end{cases}$$

The discrete distribution function $f_{hj}(\xi)$ mapped from each element I_j can be approximated by the modal basis functions and their modal coefficients \tilde{f}_j^k up to order p in the physical dimension using

$$f_{hj}(\xi) = \sum_{k=0}^p \tilde{f}_j^k \psi^k(\xi) + O(\Delta z^{p+1}) \quad (3.9)$$

where the subscript j and superscript k denote that the modal coefficient is for element I_j and modal basis function of order k respectively.

Equation (3.9) with the discrete distribution function restricted at Gauss points ξ_g can be projected onto the local space $\tilde{F}(\xi)$ of modal basis functions for each order $l \leq p$

$$\int_{-1}^1 f_{hj}(\xi_g) \psi^l(\xi_g) d\xi = \int_{-1}^1 \sum_{k=0}^p \tilde{f}_j^k \psi^k(\xi_g) \psi^l(\xi_g) d\xi \quad (3.10)$$

After simplifying by orthogonality in equation (3.7), the modal coefficients \tilde{f}_j^l for each $l \leq p$ can be evaluated from the discrete distribution function using Gaussian

quadrature ¹

$$\tilde{f}_j^l = \frac{2l+1}{2} \sum_g w_g f_{hj}(\xi_g) \psi^l(\xi_g) \quad (3.11)$$

3.1.3 Initialization of distribution function

To initialize the distribution function, the initial distribution function of the Couette flow from equations (2.11) and (2.12) is restricted at all the Gauss points in the physical space. The number of Gauss points to be taken in each element is $p + 1$, where p is the order of approximation in the physical dimension. Taking $p + 1$ points ensures that the discrete distribution function f_h is approximated at least to the order of p , and using Gauss points enables integration with high-order Gaussian quadrature. By transforming z to ξ , the value of the initial distribution function at a Gauss point ξ_g in a reference element $\xi \in [-1, 1]$ mapped from an element I_j ,

$$f_{hj}(\xi_g, 0) = f \left(z_j + \xi_g \frac{\Delta z}{2}, 0 \right) \quad (3.12)$$

The initial distribution function that is restricted at the Gauss points can be converted to modal coefficients with equation (3.11).

3.1.4 Discretized collisionless Boltzmann equation

The weak form of the nondimensional collisionless Boltzmann equation is constructed by weighted residual in each element, for all $\phi \in F(I_j)$,

$$\int_{I_j} \phi(z) \left(\frac{\partial f}{\partial t} + \frac{\sqrt{\pi}}{2} v_z \frac{\partial f}{\partial z} \right) dz = 0 \quad (3.13)$$

$$\int_{I_j} \phi(z) \frac{\partial f}{\partial t} dz + \frac{\sqrt{\pi}}{2} v_z \int_{I_j} \phi(z) \frac{\partial f}{\partial z} dz = 0 \quad (3.14)$$

¹The Gauss points ξ_g , the corresponding Gauss weights w_g , and the Gaussian quadrature algorithm are presented in appendix A

Integrate the second integral by parts

$$\int_{I_j} \phi(z) \frac{\partial f}{\partial t} dz + \frac{\sqrt{\pi}}{2} v_z \left(- \int_{I_j} \frac{d\phi(z)}{dz} f(z) dz + \phi(z) h(f^-, f^+) \Big|_{z_j - \frac{1}{2}}^{z_j + \frac{1}{2}} \right) = 0 \quad (3.15)$$

where

- superscripts $-$ and $+$ of f denotes if it is to the left or right of the element boundary respectively
- $h(\cdot, \cdot)$ is a function that calculates the flux at the element boundary given the discontinuous distribution functions to the left and right of the boundary

Since $\frac{\sqrt{\pi}}{2} v_z$ in the nondimensional collisionless Boltzmann equation is a constant in z , the flux function is an upwind flux

$$h(f^-, f^+) = \begin{cases} f^- & \text{if } \frac{\sqrt{\pi}}{2} v_z \geq 0 \\ f^+ & \text{if } \frac{\sqrt{\pi}}{2} v_z < 0 \end{cases} \quad (3.16)$$

The weak form in equation (3.15), defined for each element I_j with dimension z , can be transformed to the reference element with dimension ξ for each order $l \leq p$ of Legendre polynomial ψ^l

$$\int_{-1}^1 \psi^l(\xi) \frac{\partial f(\xi)}{\partial t} d\xi \frac{dz}{d\xi} + \frac{\sqrt{\pi}}{2} v_z \left(- \int_{-1}^1 \frac{d\psi^l(\xi)}{d\xi} \frac{d\xi}{dz} f(\xi) d\xi \frac{dz}{d\xi} + \psi^l(\xi) h(f^-, f^+) \Big|_{-1}^1 \right) = 0 \quad (3.17)$$

This can be simplified and expressed in terms of modal coefficients \tilde{f}_j^l for each order $l \leq p$ with equation (3.11). The f^+ and f^- in the flux term can also be simplified by the boundary values of Legendre polynomials of equation (3.6)

$$\sum_{k=0}^p \left[\int_{-1}^1 \psi^l(\xi) \frac{\partial \tilde{f}_j^k}{\partial t} \psi^k(\xi) d\xi \frac{dz}{d\xi} + \frac{\sqrt{\pi}}{2} v_z \left(- \int_{-1}^1 \frac{d\psi^l(\xi)}{d\xi} \tilde{f}_j^k \psi^k(\xi) d\xi + h \left(\tilde{f}_j^k, (-1)^k \tilde{f}_{j+1}^k \right) - (-1)^l h \left(\tilde{f}_{j-1}^k, (-1)^k \tilde{f}_j^k \right) \right) \right] = 0 \quad (3.18)$$

The above equation can be simplified further because of the orthogonality of the Legendre polynomials from equations (3.7) and (3.8), and derivatives from equation

(3.3). For each order l ,

$$\begin{aligned} \frac{\Delta z}{2l+1} \frac{\partial \tilde{f}_j^l}{\partial t} + \frac{\sqrt{\pi}}{2} v_z \left[\sum_{k=0}^p \left(h \left(\tilde{f}_j^k, (-1)^k \tilde{f}_{j+1}^k \right) \right. \right. \\ \left. \left. - (-1)^l h \left(\tilde{f}_{j-1}^k, (-1)^k \tilde{f}_j^k \right) \right) - \sum_m 2\tilde{f}_j^m \right] = 0 \end{aligned} \quad (3.19)$$

where $m = \begin{cases} l-1, l-3, \dots, 1 & \text{if } l \text{ is even} \\ l-1, l-3, \dots, 0 & \text{if } l \text{ is odd} \end{cases}$

With equation (3.19), the time derivative of the modal coefficients can be formed

$$\frac{\partial \tilde{f}_j^l}{\partial t} = \frac{\sqrt{\pi}}{2} v_z \frac{2l+1}{\Delta z} \left[\sum_m 2\tilde{f}_j^m + \sum_{k=0}^p \left((-1)^l h \left(\tilde{f}_{j-1}^k, (-1)^k \tilde{f}_j^k \right) - h \left(\tilde{f}_j^k, (-1)^k \tilde{f}_{j+1}^k \right) \right) \right] \quad (3.20)$$

This equation is the nondimensional collisionless Boltzmann equation discretized in the physical space by the discontinuous Galerkin method in terms of modal coefficients of Legendre polynomials which act as modal basis functions. The same equation applies for all elements I_j in the physical space except for the boundary elements. The left boundary element has the following equation

$$\frac{\partial \tilde{f}_j^l}{\partial t} = \frac{\sqrt{\pi}}{2} v_z \frac{2l+1}{\Delta z} \left[\sum_m 2\tilde{f}_j^m + (-1)^l h \left(f_{l\text{w}}, \sum_{k=0}^p (-1)^k \tilde{f}_j^k \right) - \sum_{k=0}^p h \left(\tilde{f}_j^k, (-1)^k \tilde{f}_{j+1}^k \right) \right] \quad (3.21)$$

while the right boundary element has the following equation

$$\frac{\partial \tilde{f}_j^l}{\partial t} = \frac{\sqrt{\pi}}{2} v_z \frac{2l+1}{\Delta z} \left[\sum_m 2\tilde{f}_j^m + (-1)^l h \left(\sum_{k=0}^p \tilde{f}_{j-1}^k, f_{r\text{w}} \right) - \sum_{k=0}^p h \left(\tilde{f}_j^k, (-1)^k \tilde{f}_{j+1}^k \right) \right] \quad (3.22)$$

Instead of using different equations (3.21) and (3.22) for the boundary elements, special “wall” elements can be added to the physical space so that the same equation (3.20) applies for all elements in the physical space. The modal coefficients of the “wall” elements do not change according to the discretized equation, but they only change according to the boundary conditions of the distribution function. This greatly

simplifies the implementation. The modal coefficients of the “wall” elements are

$$\begin{aligned}
\tilde{f}_{lw}^0 &= f_{lw} \\
\tilde{f}_{lw}^l &= 0 \quad \forall l > 0 \\
\tilde{f}_{rw}^0 &= f_{rw} \\
\tilde{f}_{rw}^l &= 0 \quad \forall l > 0
\end{aligned} \tag{3.23}$$

From equation (3.20), the time derivative of the modal coefficients of all orders $0 \leq l \leq p$ for each element I_j can be expressed as a linear function \tilde{L}_j of modal coefficients

$$\frac{\partial \tilde{f}_j}{\partial t} = \tilde{L}_j(\tilde{f}_i) \tag{3.24}$$

where \tilde{f}_i denotes all the modal coefficients in element I_i , $i = j - 1, j$ and $j + 1$.

This equation (3.24) also means that the time derivative of modal coefficients for the whole physical space z can be written as a linear function

$$\frac{\partial \tilde{f}}{\partial t} = \tilde{L}(\tilde{f}) \tag{3.25}$$

The time derivative of the modal coefficients of each element in equation (3.24) is a linear function with a stencil that only includes the element itself and its left or right neighbor. By combining equations (3.20) and (3.24), two constant matrices \mathbf{L}_j^+ and \mathbf{L}_j^- , each of size $(p+1) \times 2(p+1)$, can be formed for every element I_j . The same matrices \mathbf{L}_j^+ and \mathbf{L}_j^- can be used for any element, for any node in velocity space, and at any time instant.

$$\frac{\partial \tilde{f}_j}{\partial t} = \tilde{L}_j(\tilde{f}_i) = \begin{cases} \frac{\sqrt{\pi}}{2\Delta z} v_z \mathbf{L}_j^+ \cdot \begin{pmatrix} \tilde{f}_{j-1} \\ \tilde{f}_j \end{pmatrix} & \text{if } \frac{\sqrt{\pi}}{2} v_z \geq 0 \\ \frac{\sqrt{\pi}}{2\Delta z} v_z \mathbf{L}_j^- \cdot \begin{pmatrix} \tilde{f}_j \\ \tilde{f}_{j+1} \end{pmatrix} & \text{if } \frac{\sqrt{\pi}}{2} v_z < 0 \end{cases} \tag{3.26}$$

For example, for $p = 3$,

$$\begin{aligned}
& \mathbf{L}_j^- \cdot \begin{pmatrix} \tilde{f}_j \\ \tilde{f}_{j+1} \end{pmatrix} \\
= & \begin{pmatrix} 1 & 0 & 0 & 0 \\ 0 & 3 & 0 & 0 \\ 0 & 0 & 5 & 0 \\ 0 & 0 & 0 & 7 \end{pmatrix} \left[+ \begin{pmatrix} 0 & 0 & 0 & 0 \\ 2 & 0 & 0 & 0 \\ 0 & 2 & 0 & 0 \\ 2 & 0 & 2 & 0 \end{pmatrix} \right] \cdot \begin{pmatrix} \tilde{f}_j^0 \\ \tilde{f}_j^1 \\ \tilde{f}_j^2 \\ \tilde{f}_j^3 \\ \tilde{f}_{j+1}^0 \\ \tilde{f}_{j+1}^1 \\ \tilde{f}_{j+1}^2 \\ \tilde{f}_{j+1}^3 \end{pmatrix} \\
& \hspace{15em} (3.27)
\end{aligned}$$

$$\begin{aligned}
& \mathbf{L}_j^+ \cdot \begin{pmatrix} \tilde{f}_{j-1} \\ \tilde{f}_j \end{pmatrix} \\
= & \begin{pmatrix} 1 & 0 & 0 & 0 \\ 0 & 3 & 0 & 0 \\ 0 & 0 & 5 & 0 \\ 0 & 0 & 0 & 7 \end{pmatrix} \left[+ \begin{pmatrix} 0 & 0 & 0 & 0 \\ 2 & 0 & 0 & 0 \\ 0 & 2 & 0 & 0 \\ 2 & 0 & 2 & 0 \end{pmatrix} \right] \cdot \begin{pmatrix} \tilde{f}_{j-1}^0 \\ \tilde{f}_{j-1}^1 \\ \tilde{f}_{j-1}^2 \\ \tilde{f}_{j-1}^3 \\ \tilde{f}_j^0 \\ \tilde{f}_j^1 \\ \tilde{f}_j^2 \\ \tilde{f}_j^3 \end{pmatrix} \\
& \hspace{15em} (3.28)
\end{aligned}$$

3.2 Runge-Kutta time discretization

Two classes of Runge-Kutta time discretization schemes are used in this work. One is the strong stability preserving (SSP) Runge-Kutta method [11]. This class of time

Table 3.1: CFL numbers for RK3ssp for polynomials of order p

p	0	1	2	3	4	5	6
c	1.256	0.409	0.209	0.130	0.089	0.066	0.051

discretization schemes is specially developed to ensure stability for high-order time discretization provided the Courant-Friedrichs-Levy (CFL) condition is satisfied

$$\Delta t \leq c \Delta z \frac{2}{|v_z| \sqrt{\pi}} \quad (3.29)$$

where c is the CFL number, and the first-order forward Euler time discretization must be stable

$$\left\| \tilde{f} + \Delta t \tilde{L}(\tilde{f}) \right\| \leq \left\| \tilde{f} \right\| \quad (3.30)$$

The CFL numbers are different for various orders of polynomials and time discretization scheme orders, as shown in [10]. The CFL numbers for the third-order SSP Runge-Kutta (RK3ssp) method used here are shown in table 3.1.

The following is the algorithm of RK3ssp for advancing one time step Δt_k from t_k to t_{k+1}

$$\begin{aligned} \tilde{f}^{(1)} &= \tilde{f}(t_k) + \Delta t_k \tilde{L}(\tilde{f}(t_k)) \\ \tilde{f}^{(2)} &= \frac{3}{4} \tilde{f}(t_k) + \frac{1}{4} \left(\tilde{f}^{(1)} + \Delta t_k \tilde{L}(\tilde{f}^{(1)}) \right) \\ \tilde{f}(t_{k+1}) &= \frac{1}{3} \tilde{f}(t_k) + \frac{2}{3} \left(\tilde{f}^{(2)} + \Delta t_k \tilde{L}(\tilde{f}^{(2)}) \right) \end{aligned} \quad (3.31)$$

The other time discretization scheme is the commonly used classical fourth-order Runge-Kutta (RK4std) scheme [8]. Although it is not specially developed for the RKDG method, this scheme is well-known for its stability and robustness for non-linear problems. The following is the RK4std algorithm

$$\begin{aligned} \tilde{f}^{(1)} &= \tilde{L} \left(\tilde{f}(t_k) \right) \\ \tilde{f}^{(2)} &= \tilde{L} \left(\tilde{f}(t_k) + \frac{\Delta t_k}{2} \tilde{f}^{(1)} \right) \end{aligned}$$

$$\begin{aligned}
\tilde{f}^{(3)} &= \tilde{L} \left(\tilde{f}(t_k) + \frac{\Delta t_k}{2} \tilde{f}^{(2)} \right) \\
\tilde{f}^{(4)} &= \tilde{L} \left(\tilde{f}(t_k) + \Delta t_k \tilde{f}^{(3)} \right) \\
\tilde{f}(t_{k+1}) &= \tilde{f}(t_k) + \frac{\Delta t_k}{6} \left(\tilde{f}^{(1)} + 2\tilde{f}^{(2)} + 2\tilde{f}^{(3)} + \tilde{f}^{(4)} \right)
\end{aligned} \tag{3.32}$$

The RK3ssp algorithm is accurate to $O(\Delta t^3)$, while the RK4std algorithm is accurate to $O(\Delta t^4)$.

3.3 Slope limiter

A problem with numerical methods for hyperbolic systems is the occurrence of oscillations near discontinuities. As the order p of polynomial approximation increases, the magnitudes and wavelengths of the oscillations increase and decrease respectively. When the oscillations get large in magnitude, the numerical scheme can become unstable. For the RKDG method on discontinuous problems, slope limiters are often applied at every intermediate Runge-Kutta stage to ensure stability. Slope limiters are a group of numerical schemes that restrict the variations in the solution after advancing in time to ensure stability.

One slope limiter scheme that retains high-order accuracy in physical space is the Total Variational Bounded (TVB) limiter developed in [19]. The TVB limiter for approximation order $p = 2$ has also been briefly described in [10]. The advantage of the TVB limiter is that there is a rigorous proof of its total variational boundedness, thus proving the stability of the scheme

$$\sum_j |f_{j+1} - f_j|_{t_{k+1}} \leq \sum_j |f_{j+1} - f_j|_{t_k} + B\Delta t \tag{3.33}$$

where B is a constant.

The problem with the TVB limiter is that the stencil expands with p . If the high-order accuracy is to be retained, the stencil has to extend from I_{j-p+1} to I_{j+p-1} , containing a total of $2p - 1$ elements.

Another slope limiter that works well is the moment limiter developed in [7]. It keeps the k th moment monotone by keeping the order k modal coefficients \tilde{f}_j^k monotone on neighboring elements. To keep \tilde{f}_j^k monotone, we limit \tilde{f}_j^{k+1} using

$$\tilde{f}_j^{k+1} = \text{minmod} \left(\tilde{f}_j^{k+1}, \frac{\tilde{f}_{j+1}^k - \tilde{f}_j^k}{2k+1}, \frac{\tilde{f}_j^k - \tilde{f}_{j-1}^k}{2k+1} \right) \quad (3.34)$$

where

$$\text{minmod}(a, b, c) = \begin{cases} \text{sign}(a) \min(|a|, |b|, |c|) & \text{if } \text{sign}(a) = \text{sign}(b) = \text{sign}(c) \\ 0 & \text{otherwise} \end{cases} \quad (3.35)$$

One problem with the moment limiter is that when a discontinuity is close in distance (of the order of element size Δz) to a local extrema, the high-order accuracy in physical space is often lost around the local extrema and this effect of losing accuracy spreads far from both the discontinuity and local extrema. More about this problem is illustrated in section 5.6. The generalized moment limiter described in the next section does not have this problem of losing accuracy.

3.3.1 Generalized moment limiter

In this thesis, a slope limiter scheme called the generalized moment limiter has been developed. The generalized moment limiter has the flexibility of retaining the high-order in physical space up to the desired order k , depending on the maximum $\frac{d^k f}{dz^k}$ which can be specified as a parameter. It also has a stencil that is limited to its closest neighbors, to elements I_{j-1} , I_j and I_{j+1} . The generalized moment limiter is based on the idea of keeping the moments monotone, as given in the moment limiter [7], with modifications to relax the restrictions for high-order smooth solutions, inspired by the generalized minmod function in the TVB limiter [19].

The generalized moment limiter restricts the oscillations to within the limits of the specified parameters $M(k)$. The problem with the generalized moment limiter now, just like the moment limiter, is that there is no mathematical proof to show the

stability of the scheme.

The generalized slope limiter scheme is shown in the following

```

for all  $I_j$ 
  for  $k = p - 1, \dots, 0$ 
    if  $|\tilde{f}_j^{k+1}| < M(k + 1)$ 
      break
    else
       $m = \text{minmod} \left( (2k + 1)\tilde{f}_j^{k+1}, \tilde{f}_{j+1}^k - \tilde{f}_j^k, \tilde{f}_j^k - \tilde{f}_{j-1}^k \right)$ 
      if  $m = (2k + 1)\tilde{f}_j^{k+1}$ , break
      else  $(2k + 1)\tilde{f}_j^{k+1} = m$  end
    end
  end
end

```

Now, we specify the parameter $M(k)$ for each order $k \leq p$. Let $d(k) = \max_z \left| \frac{d^k f(z)}{dz^k} \right|$. $d(k)$ is the maximum k^{th} derivative of f . For example, for $f(z) = -0.2 \sin(2\pi z)$, $d_{\sin}(k) = \max_z \left| \frac{d^k f(z)}{dz^k} \right| = 0.2(2\pi)^k$. We convert $d(k)$ to be in terms of modal coefficients

$$\begin{aligned}
d(k) &= \max_z \left| \frac{d^k f(z)}{dz^k} \right| \\
&= \max_{\xi, \text{all } j} \left| \sum_{k=0}^p \tilde{f}_j^k \frac{d^k}{d\xi^k} \psi^k(\xi) \left(\frac{d\xi}{dz} \right)^k \right| \\
&= \max_{\xi, \text{all } j} \left| \tilde{f}_j^k \right| \frac{d^k}{d\xi^k} \psi^k(\xi) \left(\frac{2}{\Delta z_j} \right)^k \\
\max_{\xi, \text{all } j} \left| \tilde{f}_j^k \right| &= \frac{d(k)}{\frac{d^k}{d\xi^k} \psi^k(\xi) \left(\frac{2}{\Delta z_j} \right)^k} \tag{3.36}
\end{aligned}$$

The maximum modal coefficient of order k is fixed as the parameter $M(k)$

$$M(k) = \frac{d(k)}{\frac{d^k}{d\xi^k} \psi^k(\xi) \left(\frac{2}{\Delta z_j} \right)^k} \tag{3.37}$$

The parameter $M(k)$ endows the generalized moment limiter user the flexibility to control the degree of oscillation limiting. The smaller the $M(k)$, the larger the degree of oscillation limiting. To remove all oscillations, one can set $M(k) = 0$ for all orders $k \leq p$; this is equivalent to the moment limiter scheme. On the other hand, if no limiting is required, one can set $M(k) \rightarrow \infty$ to effectively switch the oscillation limiting off.

The generalized moment limiter is more efficient than the moment limiter because it stops checking element I_j once a modal coefficient \tilde{f}_j^k satisfies $|\tilde{f}_j^k| < M(k)$, starting from highest order $k = p$ to lowest order 1. It also retains the high-order accuracy in the smooth regions of the expected solution when the parameter $M(k)$ is set correctly.

3.3.2 Viscosity limiter

A different approach to slope limiting is to add a viscosity to discontinuous regions as developed in [16, 15], inspired by early methods described in [14]. The idea behind the viscosity approach is to add a dissipative model term to the original equation which, in our case, is the collisionless Boltzmann equation

$$\frac{\partial f}{\partial t} + \frac{\sqrt{\pi}}{2} v_z \left(\frac{\partial f}{\partial z} - \nu \frac{\partial^2 f}{\partial z^2} \right) = 0 \quad (3.38)$$

where ν controls the amount of viscosity added.

In order to solve the above equation, the local discontinuous Galerkin (LDG) method described in [9] is used. The LDG method is only used in elements with non-zero viscosity, in other words, in elements in which there are significant oscillations. The amount of oscillations in an element I_j in physical space is estimated by the following smoothness indicator

$$s_j = \frac{\int_{-1}^1 \left(f_{hj}(\xi) - \hat{f}_{hj}(\xi) \right)^2 d\xi}{\int_{-1}^1 \left(f_{hj}(\xi) \right)^2 d\xi} \quad (3.39)$$

where f_{hj} is the approximate solution in element I_j determined by equation (3.9),

and \hat{f}_{hj} is a truncated expansion of the same solution

$$\hat{f}_{hj}(\xi) = \sum_{k=0}^{p-1} \tilde{f}_j^k \psi^k(\xi) + O(\Delta z^p) \quad (3.40)$$

The amount of viscosity ν_j added to each element is then determined by the following function

$$\nu_j = \begin{cases} 0 & \text{if } s_j < \bar{s} \\ \nu_0 \frac{\Delta z}{p} & \text{if } s_j \geq \bar{s} \end{cases} \quad (3.41)$$

where \bar{s} is the mean of s_j over the whole physical space, and ν_0 is the viscosity parameter chosen empirically to sufficiently limit oscillations without degrading the solution.

The smoothness indicator can be efficiently evaluated by Gaussian quadrature. Since the more expensive LDG is only done in a few “non-smooth” elements near the discontinuities, the viscosity limiter is computationally inexpensive.

3.4 Implementation

The RKDG method has been implemented in both Matlab and C. The implementations are similar. In the C version, several linear algebraic functions have been written with the help of [17]. The C version is mainly for:

- Testing the program for arbitrary precisions, which is given in a C++ library Arprec [2]. This is to eliminate the effect of precision errors on the convergence tests.
- Integration with the collision integral evaluator, which has been coded in C++ [4].

The following is the RKDG algorithm for the collisionless Boltzmann equation for one node in the velocity space:

1. Initialize by evaluating the discrete distribution function f_h at all Gauss points

in physical space with equations (2.11), (2.12) and (3.12). For order p approximation in the physical dimension, each element requires $p + 1$ Gauss points.

2. Generate the matrices \mathbf{L}^+ and \mathbf{L}^- according to equations (3.20) and (3.26).
3. Convert the distribution function at the Gauss points to modal coefficients \tilde{f}_j^l for all orders $l = 0$ to p in every element I_j using equation (3.11).
4. Evaluate the time derivative of the modal coefficients $\frac{d\tilde{f}_j^l}{dt}$ for every element I_j and order $l \leq p$ with equation (3.26).
5. Advance in time and update the modal coefficients with the chosen Runge-Kutta time discretization scheme. The time derivative of the modal coefficients must be re-evaluated for each intermediate stage. If necessary, limit the change in the modal coefficients with a slope limiter from section 3.3 for every intermediate stage.
6. Convert the updated modal coefficients in each element at the desired time instant to approximate solutions at the desired physical space positions with equation (3.9).
7. Repeat steps 4 to 6 if an approximate solution at a new time instant is desired.

3.5 Error measurement

The numerical error is measured in two ways. The first way is an L1 norm of the difference between the numerical solution and the analytical solution at N discrete points in the domain,

$$\|\varepsilon\|_1 = \frac{1}{N} \sum_N |f_{\text{numeric}} - f_{\text{analytic}}| \quad (3.42)$$

The second way is an L-infinity norm of the difference between the numerical solution and analytical solution at the same N discrete points in the domain

$$\|\varepsilon\|_\infty = \max_N |f_{\text{numeric}} - f_{\text{analytic}}| \quad (3.43)$$

Chapter 4

A test problem with continuous solutions

In this section we investigate the ability of the RKDG method to provide high-order accuracy to problems with continuous solutions. Our objective is to verify that the theoretically predicted convergence rates both for physical space and time discretizations can be obtained. For these tests a simple test problem is used; this is described in the next section. Convergence behavior for discontinuous solutions is discussed in the next chapter.

4.1 The test problem

Consider a simple system $z \in [0, 1]$ where $f = f(z, t)$ with $v_z = \frac{2}{\sqrt{\pi}}$ leading to a simple “Boltzmann equation”

$$\frac{\partial f}{\partial t} + \frac{\partial f}{\partial z} = 0 \tag{4.1}$$

and a time dependent boundary condition

$$f_{1w} = f(0, t) = 0.2 \sin(2\pi t) \tag{4.2}$$

The analytical solution is given by

$$f(z, t) = 0.2 \sin(2\pi(t - z)) \quad (4.3)$$

which is continuous for all z , provided sufficient time is allowed for the solution to reach steady state, or the initial distribution is chosen as

$$f(z, 0) = -0.2 \sin(2\pi z) \quad (4.4)$$

Below, we describe the RKDG solution method of this problem and extensive investigation of the convergence rate of this method to the analytical solution given above.

4.2 Discontinuous Galerkin discretization

The physical space discretization of the continuous problem with the discontinuous Galerkin method is similar to that shown in section 3.1. The same physical space elements I_j , reference elements and Legendre polynomials $\psi^l(\xi)$ as modal basis functions, like those given in sections 3.1.1 and 3.1.2, are used.

The initialization of the sine function is also similar to the procedure shown in section 3.1.3. The initial distribution function $f(z, 0)$ is restricted in every element I_j and mapped to discrete Gauss points in the reference element to give the discrete distribution function $f_{hj}(\xi, 0)$ by equation (3.12). If p is the order of approximation in the physical dimension, the number of Gauss points in each element is $p + 1$. The discrete distribution function $f_{hj}(\xi, 0)$ is expressed in terms of modal coefficients \tilde{f}_j^l of the modal basis functions with equation (3.11).

From the simple governing PDE of this problem in equation (4.1), the distribution function translates only in the positive z direction. The flux function of equation (3.16) only takes the left value

$$h(f^-, f^+) = f^- \quad (4.5)$$

The derivation of the discretized nondimensional collisionless Boltzmann equation has been given in section 3.1.4. The discretized nondimensional collisionless Boltzmann equation for this continuous problem is

$$\frac{\partial \tilde{f}_j^l}{\partial t} = \frac{2l+1}{\Delta z} \left[\sum_m 2\tilde{f}_j^m + \sum_{k=0}^p \left((-1)^l \tilde{f}_{j-1}^k - \tilde{f}_j^k \right) \right] \quad (4.6)$$

$$\text{where } m = \begin{cases} l-1, l-3, \dots, 1 & \text{if } l \text{ is even} \\ l-1, l-3, \dots, 0 & \text{if } l \text{ is odd} \end{cases}$$

Since the distribution function translates only in the positive z direction, only the left “wall” element needs to be added. The left boundary distribution changes with time as in equation (4.2), so the order 0 modal coefficient of the left “wall” element also changes with time

$$\begin{aligned} \tilde{f}_{1w}^0(t) &= 0.2 \sin(2\pi t) \\ \tilde{f}_{1w}^l &= 0 \quad \forall l > 0 \end{aligned} \quad (4.7)$$

The modal coefficients of non-zero order of the left “wall” element are always zeros.

The updating of the left “wall” element modal coefficients has to be done manually since the discretized nondimensional collisionless Boltzmann equation (4.6) does not change the “wall” element at all. The manual updating depends on the time discretization scheme chosen and shall be described further in section 4.3.1.

4.3 Runge-Kutta time discretization

From equation (4.6), the time derivative of the modal coefficients for each order $l \leq p$ and each element I_j can be expressed as a linear function \tilde{L} of modal coefficients,

$$\frac{\partial \tilde{f}_j^l}{\partial t} = \tilde{L}_j(\tilde{f}_i) \quad (4.8)$$

and \tilde{f}_i denotes all the modal coefficients in element I_i , $i = j-1, j$.

The time derivative of the modal coefficients of each element in equation (4.8) is a linear function with a stencil that only includes the element itself and its left neighbor. By combining equations (4.6) and (4.8), a constant matrix \mathbf{L}_j^+ of size $(p+1) \times 2(p+1)$ can be formed for every element I_j . The same matrix \mathbf{L}_j^+ can be used for all elements and at different time instants.

$$\begin{aligned} \frac{\partial \tilde{f}_j}{\partial t} &= \tilde{L}_j(\tilde{f}_i) \\ &= \frac{1}{\Delta z} \mathbf{L}_j^+ \cdot \begin{pmatrix} \tilde{f}_{j-1} \\ \tilde{f}_j \end{pmatrix} \end{aligned} \quad (4.9)$$

Equation (3.28) has shown an example of \mathbf{L}_j^+ for $p = 3$.

The two Runge-Kutta time discretization schemes tested in the continuous problem are RK3ssp and RK4std. The RK3ssp and RK4std algorithms are given in equations (3.31) and (3.32) respectively.

The time steps chosen for both RK3ssp and RK4std schemes satisfy the CFL condition

$$\Delta t \leq c \Delta z \quad (4.10)$$

with the CFL numbers c given in table 3.1. Even though this list of CFL numbers is meant for the SSP schemes, the CFL numbers have been tested in this work to be applicable to the RK4std scheme too, as long as the time steps are not too tightly bounded by the CFL condition. This means that the RK4std scheme is stable if

$$\Delta t \ll c \Delta z \quad (4.11)$$

The RK3ssp scheme is accurate to $O(\Delta t^3)$ while the RK4std algorithm is accurate to $O(\Delta t^4)$.

4.3.1 Left “wall” element

Since the order 0 modal coefficient of the left “wall” element changes with time and the left “wall” element is not altered by the discretized equation (4.6), the modal co-

efficients of the left “wall” element need to be updated manually at each intermediate Runge-Kutta stage.

For the RK3ssp scheme,

$$\begin{aligned}
\tilde{f}_{1w}^0(t_k) &= 0.2 \sin(2\pi t_k) \\
\tilde{f}_{1w}^{0(1)} &= 0.2 \sin(2\pi(t_k + \Delta t_k)) \\
\tilde{f}_{1w}^{0(2)} &= 0.2 \sin\left(2\pi\left(t_k + \frac{1}{2}\Delta t_k\right)\right)
\end{aligned} \tag{4.12}$$

For the RK4std scheme,

$$\begin{aligned}
\tilde{f}_{1w}^{0(1)} &= 0.2 \sin(2\pi t_k) \\
\tilde{f}_{1w}^{0(2)} &= 0.2 \sin\left(2\pi\left(t_k + \frac{1}{2}\Delta t_k\right)\right) \\
\tilde{f}_{1w}^{0(3)} &= 0.2 \sin\left(2\pi\left(t_k + \frac{1}{2}\Delta t_k\right)\right) \\
\tilde{f}_{1w}^{0(4)} &= 0.2 \sin(2\pi(t_k + \Delta t_k))
\end{aligned} \tag{4.13}$$

4.4 Implementation

This test problem has been implemented in Matlab and C with similar algorithms. The C version makes use of the C++ library Arprec [2]. Arprec allows the program to run with arbitrary precision to eliminate the effect of finite precision errors on the convergence tests.

The algorithm can be summarized as follows:

1. Initialize by evaluating the discrete sine function f_h at all the Gauss points in the physical space with equations (4.2), (4.4) and (3.12). For order p approximation in the physical dimension, each element requires $p + 1$ Gauss points.
2. Generate the matrix \mathbf{L}^+ according to equations (4.6) and (4.9).
3. Convert the discrete sine function at the Gauss points to modal coefficients \tilde{f}_j^l for all orders $l = 0$ to p in every element I_j using equation (3.11).

4. Evaluate the time derivative of the modal coefficients $\frac{\partial \tilde{f}_j^l}{\partial t}$ for every element I_j and order $l \leq p$ with equation (4.9).
5. Advance in time and update the modal coefficients with the chosen Runge-Kutta time discretization scheme. The time derivative of the modal coefficients and the left “wall” element modal coefficients must be re-evaluated for each intermediate stage as shown in section 4.3.1.
6. Convert the updated modal coefficients in each element at the desired time instant to approximate solutions at the desired physical space positions with equation (3.9).
7. Repeat steps 4 to 6 if an approximate solution at a new time instant is desired.

4.5 Error convergence

The analytical solution of this problem is given by equation (4.3). The numerical error is measured at $t = 1$ against the analytical solution in the L1 and L-infinity norm at 9 equispaced nodes per element ($N = 9n$). The range of n (number of elements in the physical space z , and $n = 1/\Delta z$) tested in all cases is $n = 10, 20, 40, 80$ and 160 . The L1 and L-infinity norms are defined in section 3.5.

In the first case, using RK3ssp, the parameters are:

- Time step $\Delta t = 10^{-4}$
- Integrating in time from $t = 0$ to 1 with RK3ssp
- Order of approximation p varies from 1 to 6

The numerical errors are shown in table 4.1 and figure 4-1. The numerical solution exhibits a convergence rate of approximately $O(\Delta z^{p+1})$ before the errors saturate at smaller Δz values. The error saturation at small Δz values is due to time discretization as we show below.

In the second case, the RK4std method is used. The parameters are:

- Time step $\Delta t = 10^{-4}$
- Integrating in time from $t = 0$ to 1 with RK4std
- Order of approximation p varies from 1 to 6

The numerical errors are shown in table 4.2 figure 4-2. The numerical solution converges with a rate of $O(\Delta z^{p+1})$ before saturating at smaller Δz values.

The first two cases have demonstrated that the RKDG method is accurate to $O(\Delta z^{p+1})$, provided the timestep is sufficiently small for time discretization error to be negligible. Investigation of the convergence rate is complicated by the fact that numerical precision introduces a limit on the smallest error that can be detected. For this reason, we use an arbitrary precision routine for this test, as explained in the next section.

4.5.1 Arbitrary precision calculations

By default, MATLAB represents floating-point numbers in double-precision [12]. The C++ library Arprec can be utilized to increase the precision of the floating-point numbers and hence decrease the effect of precision error. Thus, for the time discretization convergence test we have used this library in conjunction with the C version of the RKDG code.

Since the L1 and L-infinity norms have been shown to be equivalent above, only one of the norms (L1) will be used here. The solution parameters are:

- Varying time step $t = 10^{-3}, 10^{-4}$ and 10^{-5} .
- Integrating in time from $t = 0$ to 1 with RK3ssp and RK4std
- Order of approximation $p = 5$
- In Arprec, number of precision digits is 100

The resulting numerical errors are shown in figure 4-3 and the error saturation levels are listed in table 4.3.

The RK3ssp method is able to maintain stability for a finer physical space discretization Δz than the RK4std method. At $\Delta t = 10^{-3}$, RK3ssp is still stable for $\Delta z = 1/80$ while RK4std is no longer stable for $\Delta z < 1/40$. Being able to use a smaller Δz for the same timestep Δt is advantageous for RK3ssp because it means that higher-order accuracy in physical space can be achieved without decreasing Δt . Using smaller Δt means taking more iterations before reaching the required time instant.

The error saturation levels with varying Δt show a convergence of $O(\Delta t^3)$ for the RK3ssp time discretization scheme. The error saturation levels with varying Δt show a convergence of $O(\Delta t^4)$ for the RK4std method. This convergence behavior verifies that the RKDG method exhibits the expected order of accuracy in time.

(a) $\|\varepsilon\|_1$

(b) $\|\varepsilon\|_\infty$

Figure 4-1: $\|\varepsilon\|$ against Δz for $\Delta t = 10^{-4}$ using RK3ssp

(a) $\|\varepsilon\|_1$

(b) $\|\varepsilon\|_\infty$

Figure 4-2: $\|\varepsilon\|$ against Δz for $\Delta t = 10^{-4}$ using RK4std

(a) RK3ssp

(b) RK4std

Figure 4-3: $\|\varepsilon\|_1$ against Δt for $p = 5$, with Arprec 100 precision digits

Table 4.1: Convergence with respect to Δz for $\Delta t = 10^{-4}$ using RK3ssp

p	$\frac{1}{\Delta z}$	$\ \varepsilon\ _1$		$\ \varepsilon\ _\infty$	
		$10^{10}\ \varepsilon\ $	order	$10^{10}\ \varepsilon\ $	order
1	10	30607341.94	-	91342810.76	-
	20	6867810.03	2.16	24593003.02	1.89
	40	1629806.55	2.08	6306877.18	1.96
	80	398193.88	2.03	1597301.47	1.98
	160	98421.33	2.02	401936.97	1.99
2	10	1221446.86	-	4402228.55	-
	20	152337.80	3.00	567249.93	2.96
	40	18931.96	3.00	71398.77	2.99
	80	2363.03	3.00	8939.32	3.00
	160	295.27	3.00	1117.80	3.00
3	10	47716.46	-	127141.34	-
	20	2948.66	4.02	7864.23	4.01
	40	183.76	4.00	496.15	3.99
	80	11.47	4.00	31.06	4.00
	160	0.71	4.01	1.91	4.02
4	10	1171.55	-	4587.98	-
	20	37.12	4.98	147.94	4.95
	40	1.16	5.00	4.57	5.02
	80	0.07	3.98	0.20	4.48
	160	0.06	0.20	0.13	0.67
5	10	37.40	-	97.56	-
	20	0.58	6.00	1.50	6.02
	40	0.06	3.16	0.14	3.41
	80	0.06	0.02	0.13	0.14
	160	0.06	0.00	0.13	0.00
6	10	0.87	-	3.06	-
	20	0.06	3.76	0.14	4.41
	40	0.06	0.02	0.13	0.18
	80	0.06	0.00	0.13	0.00
	160	0.06	0.00	0.13	0.00

Table 4.2: Convergence with respect to Δz for $\Delta t = 10^{-4}$ using RK4std

p	$\frac{1}{\Delta z}$	$\ \varepsilon\ _1$		$\ \varepsilon\ _\infty$	
		$10^{13}\ \varepsilon\ $	order	$10^{13}\ \varepsilon\ $	order
1	10	30607341911.68	-	91342810777.46	-
	20	6867810004.22	2.16	24593003030.28	1.89
	40	1629806537.32	2.08	6306877206.66	1.96
	80	398193864.83	2.03	1597301499.72	1.98
	160	98421315.91	2.02	401937006.91	1.99
2	10	1221446851.08	-	4402228630.61	-
	20	152337794.57	3.00	567245001.65	2.96
	40	18931957.74	3.01	71398841.08	2.99
	80	2363028.68	3.00	8939381.63	3.00
	160	295266.98	3.00	1117861.13	3.00
3	10	47716456.72	-	127141353.71	-
	20	2948662.72	4.02	7864240.42	4.01
	40	183767.52	4.00	496168.89	3.99
	80	11477.27	4.00	31083.30	4.00
	160	717.20	4.00	1943.85	4.00
4	10	1171553.11	-	4587949.49	-
	20	37119.66	4.98	148030.22	4.95
	40	1152.90	5.01	4653.49	4.99
	80	35.96	5.00	145.25	5.00
	160	1.12	5.00	4.54	5.00
5	10	37397.59	-	97576.21	-
	20	578.50	6.01	1508.84	6.02
	40	9.02	6.00	23.82	5.99
	80	0.14	5.97	0.73	5.04
	160	0.01	3.35	1.46	-1.01
6	10	871.63	-	2946.09	-
	20	7.00	6.96	23.91	6.95
	40	0.06	6.98	0.23	6.68
	80	0.02	1.77	0.45	-0.94
	160	0.01	0.22	1.06	-1.24

Table 4.3: Convergence with respect to Δt for $p = 5$, with Arprec 100 precision digits

Δt	RK3ssp			RK4std		
	$\frac{1}{\Delta z}$	$10^{14}\ \varepsilon\ _1$	order	$\frac{1}{\Delta z}$	$10^{14}\ \varepsilon\ _1$	order
10^{-3}	80	647027.46	-	40	1374.35	-
10^{-4}	160	636.05	3.01	160	0.11	4.08
10^{-5}	160	0.64	3.00	no saturation for $\frac{1}{\Delta z} \leq 160$		

THIS PAGE INTENTIONALLY LEFT BLANK

Chapter 5

A test problem with discontinuous solutions

In chapter 4 we have verified the high-order accuracy of the RKDG method for continuous solutions. In this chapter we investigate the behavior of this scheme in the presence of discontinuities. We are particularly interested in verifying the claim [10] that the RKDG method continues to exhibit high-order accuracy in both physical space and time away from discontinuities. In this chapter we also investigate the performance of slope limiters used to minimize oscillations in the vicinity of discontinuities. For this investigation we use the test problem of chapter 4, suitably modified such that a propagating discontinuity is present.

5.1 The test problem

Consider the test problem described in section 4.1, in which a sinusoidal oscillation at $z = 0$ is advected into the domain ($z > 0$) for $t > 0$. In contrast to section 4.1, however, the initial distribution is a constant function

$$f(z, 0) = -0.2 \tag{5.1}$$

Analytically, the distribution function translates in the positive z direction at the

speed of one unit per unit time. The analytical solution for the above problem is

$$f(z, t) = \begin{cases} 0.2 \sin(2\pi(t - z)) & z < t \\ -0.2 & z \geq t \end{cases} \quad (5.2)$$

which can readily be seen to be discontinuous at $z = t$.

5.2 Discontinuous Galerkin discretization

The physical space discretization of this problem is similar to that shown in section 3.1. The same physical space elements I_j , reference elements and Legendre polynomials $\psi^l(\xi)$ as modal basis functions, like those given in sections 3.1.1 and 3.1.2, are used.

The initialization of the initial constant function is very simple. The discrete distribution function is $f_{hj}(\xi, 0) = -0.2$ at Gauss points in every element I_j . If p is the order of approximation in the physical dimension, the number of Gauss points in each element is $p + 1$. The initial modal coefficients in each element I_j are

$$\begin{aligned} f_j^0(0) &= -0.2 \\ f_j^l(0) &= 0 \quad 1 \leq l \leq p \end{aligned} \quad (5.3)$$

Similarly, the flux function of equation (3.16) only takes the left value,

$$h(f^-, f^+) = f^- \quad (5.4)$$

The derivation of the discretized nondimensional collisionless Boltzmann equation has been given in section 3.1.4. The discretized nondimensional collisionless Boltzmann equation for this problem is the same as equation (4.6)

$$\frac{\partial \tilde{f}_j^l}{\partial t} = \frac{2l + 1}{\Delta z} \left[\sum_m 2\tilde{f}_j^m + \sum_{k=0}^p \left((-1)^l \tilde{f}_{j-1}^k - \tilde{f}_j^k \right) \right] \quad (5.5)$$

$$\text{where } m = \begin{cases} l - 1, l - 3, \dots, 1 & \text{if } l \text{ is even} \\ l - 1, l - 3, \dots, 0 & \text{if } l \text{ is odd} \end{cases}$$

Similar to section 4.2, the left boundary distribution changes with time as in equation (4.2) and the order 0 modal coefficient of the left “wall” element also changes with time,

$$\begin{aligned} \tilde{f}_{\text{lw}}^0(t) &= 0.2 \sin(2\pi t) \\ \tilde{f}_{\text{lw}}^l &= 0 \quad \forall l > 0 \end{aligned} \tag{5.6}$$

The modal coefficients of non-zero order of the left “wall” element are always zeros.

The time derivative of the modal coefficients for each order $l \leq p$ and each element I_j can be expressed as a linear function \tilde{L} of modal coefficients and the matrix \mathbf{L}_j^+ can be constructed by equations (5.5) and (4.9). The matrix \mathbf{L}_j^+ is the same as in the problem with continuous solution.

5.3 Runge-Kutta time discretization schemes

The Runge-Kutta time discretization schemes and the time steps are described in detail in section 4.3. We will use the time discretization scheme of RK3ssp since it has been shown to maintain stability for smaller physical space element Δz at the same time step Δt than RK4std. The RK3ssp algorithm is given in equation (3.31).

The left “wall” element is also the same as in the continuous case, and the manual updating of the modal coefficients is the same as described in section 4.3.1.

5.4 Slope limiter

In this problem, a propagating discontinuity at $z = t$ is present. Oscillations can appear in the vicinity of the discontinuity and affect the stability of the RKDG method. To ensure stability, slope limiters can be applied. The effectiveness of the moment limiter, generalized moment limiter and viscosity limiter described in section 3.3 will be tested in this problem. The limiting shall be done after every intermediate Runge-Kutta stage.

For the generalized moment limiter, the parameter $M(k)$ used is as described in section 3.3.1. For the sine function in our smooth region $f(z) = -0.2 \sin(2\pi z)$, $d_{\sin}(k) = \max_z \left| \frac{d^k f(z)}{dz^k} \right| = 0.2(2\pi)^k$ and the parameter $M(k)$ is to be calculated according to equation (3.37).

For the viscosity limiter described in 3.3.2, we fix the viscosity parameter to be $\nu_0 = 0.1$, which has been found to be sufficiently large to limit the oscillations in this problem.

5.5 Implementation

This test problem has been implemented in Matlab and C with similar algorithms:

1. Initialize the modal coefficients \tilde{f}_j^l for all orders $l = 0$ to p in every element I_j with equation (5.3).
2. Generate the matrix \mathbf{L}^+ according to equations (5.5) and (4.9).
3. Evaluate the time derivative of the modal coefficients $\frac{\partial \tilde{f}_j^l}{\partial t}$ for every element I_j and order $l \leq p$ with equation (4.9).
4. Advance in time and update the modal coefficients with the chosen Runge-Kutta time discretization scheme. The time derivative of the modal coefficients and the left “wall” element modal coefficients must be re-evaluated for each intermediate stage. If desired, limit the change in the modal coefficients with a slope limiter for every intermediate step.
5. Convert the updated modal coefficients in each element at the desired time instant to approximate solutions at the desired physical space positions with equation (3.9).
6. Repeat steps 3 to 5 if an approximate solution at a new time instant is desired.

5.6 Error convergence

The analytical solution of this problem is given by equation (5.2). We integrate in time from $t = 0$ to $t = 0.7$ so that a discontinuity is present at $z = t = 0.7$. To verify the claim that high-order accuracy is maintained away from the discontinuity, we measure the numerical error against the analytical solution in the L1 norm at 9 equispaced nodes per element within the range $0 < z < 0.2$ (N is the total number of equispaced nodes in the range $0 < z < 0.2$)

$$\|\varepsilon\|_1 = \frac{1}{N} \sum_{N, 0 < z < 0.2} |f_{\text{numeric}} - f_{\text{analytic}}| \quad (5.7)$$

The range of n (number of elements in the physical space z , and $n = 1/\Delta z$) tested in all cases is $n = 10, 20, 40, 80$ and 160 .

In the first case, the Matlab version has been tested with the following parameters:

- Time step $\Delta t = 10^{-4}$
- Integrating in time from $t = 0$ to 0.7 using RK3ssp
- Order of approximation p varies from 1 to 6
- Using no limiter, moment limiter, generalized moment limiter and viscosity limiter

The numerical solutions with no limiter, moment limiter, generalized limiter and viscosity limiter are shown in figure 5-1.

Without slope limiter, oscillations are present around the discontinuity. The oscillations propagate to three elements in front of and two elements behind the discontinuity. With the moment limiter, the oscillations have been removed from the numerical solution. However, the gradient at the discontinuity is much less steep, spreading the discontinuity over three elements. The local maximum of the sine function in the smooth region has also been flattened by the moment limiter. High-order accuracy in physical space is obviously lost at the local maximum. With the

generalized moment limiter, the magnitude of the oscillations is much smaller than without slope limiter. The oscillations still propagate to three elements in front of and two elements behind the discontinuity, but they have much lower frequencies and magnitudes. The viscosity limiter shows the best performance in terms of oscillation limiting - no oscillation is observed around the discontinuity. The gradient at the discontinuity is also steep, spreading the discontinuity over just two elements. This also shows that the viscosity limiter is computationally inexpensive, as mentioned in section 3.3.2, since there are only two “non-smooth” elements which will have added viscosity and need to be solved by the local discontinuous Galerkin (LDG) method.

The numerical errors are shown in table 5.1, 5.2 and figure 5-2.

Without slope limiter, the numerical solution away from the discontinuity exhibits a convergence rate of approximately $O(\Delta z^{p+1})$. With the moment limiter, the numerical solution shows a convergence of $O(\Delta z^{p+1})$ for $p \leq 2$, but for larger p , the convergence rate stagnates at $O(\Delta z^3)$. This is because the moment limiter, while keeping the moments monotone, has put all the modal coefficients of order $k > 2$ of the sine distribution to zero. With generalized moment limiter and viscosity limiter, the convergence rate is $O(\Delta z^{p+1})$. This verifies the high-order accuracy in physical space of the RKDG method with no slope limiter, generalized moment limiter and viscosity limiter.

The error saturation at small Δz values is due to time discretization as we show below.

5.6.1 Arbitrary precision calculations

The C version of the RKDG code is used with the Arprec library to remove the effect of finite precision, as in section 4.5.1. The solution parameters are:

- Varying time step $t = 10^{-3}$, 10^{-4} and 10^{-5} .
- Integrating in time from $t = 0$ to 0.7 with RK3ssp
- Order of approximation $p = 5$

- In Arprec, number of precision digits is 100
- Using no limiter, generalized moment limiter and viscosity limiter

The resulting numerical errors are shown in figure 5-3 and the error saturation levels are listed in table 5.3.

With the generalized moment limiter, stability is maintained for a finer physical space discretization Δz than without limiter. At $\Delta t = 10^{-3}$, it is still stable for $\Delta z = 1/160$ with the generalized moment limiter while it is no longer stable for $\Delta z < 1/40$ without limiter. The stability is only maintained for a coarser physical space discretization with viscosity limiter, as it becomes unstable for $\Delta z < 1/20$.

The error saturation levels with varying Δt show a convergence of $O(\Delta t^3)$ for the RK3ssp time discretization scheme when no slope limiter, generalized moment limiter or viscosity limiter is applied. This convergence behavior verifies that the RKDG method exhibits the expected order of accuracy in time for a discontinuous solution. Therefore, we have verified that with no slope limiter, generalized moment limiter or viscosity limiter, high-order accuracy in physical space and time for smooth regions away from the discontinuity is retained.

Among the slope limiters, the viscosity limiter shows the most promise for limiting oscillations (no oscillations visible around the discontinuity), keeping the discontinuity over a small length (two elements), and retaining high-order accuracy in both physical space and time away from discontinuities.

(a) No limiter

(b) Moment limiter

(c) Generalized moment limiter

(d) Viscosity limiter

Figure 5-1: Numerical solutions for $\Delta t = 10^{-4}$, $n = 10$ and $p = 5$ with no limiter, moment limiter, generalized moment limiter and viscosity limiter using RK3ssp

(a) No limiter

(b) Moment limiter

(c) Generalized moment limiter

(d) Viscosity limiter

Figure 5-2: $\|\varepsilon\|_1$ against Δz for $\Delta t = 10^{-4}$ with no limiter, moment limiter, generalized moment limiter and viscosity limiter using RK3ssp

(a) No limiter

(b) Generalized moment limiter

(c) Viscosity limiter

Figure 5-3: $\|\varepsilon\|_1$ against Δt for $p = 5$ with no limiter, generalized slope limiter and viscosity limiter using RK3ssp, with Arprec 100 precision digits

Table 5.1: Convergence with respect to Δz for $\Delta t = 10^{-4}$ with no limiter and moment limiter using RK3ssp

p	$\frac{1}{\Delta z}$	No limiter		Moment limiter	
		$10^9 \ \varepsilon\ _1$	order	$10^9 \ \varepsilon\ _1$	order
1	10	2049541.01	-	2364123.56	-
	20	522694.98	1.97	520897.14	2.18
	40	132273.11	1.98	132272.51	1.98
	80	33322.24	1.99	33322.24	1.99
	160	8366.04	1.99	8366.04	1.99
2	10	150654.75	-	973467.62	-
	20	18318.29	3.04	93302.63	3.38
	40	2265.73	3.02	10325.26	3.18
	80	281.93	3.01	1145.13	3.17
	160	35.17	3.00	126.23	3.18
3	10	3839.79	-	860773.47	-
	20	245.61	3.97	94802.37	3.18
	40	15.58	3.98	10091.97	3.23
	80	0.98	4.00	1053.26	3.26
	160	0.07	3.88	105.26	3.32
4	10	146.54	-	860765.89	-
	20	4.45	5.04	94665.11	3.18
	40	0.14	4.96	9936.82	3.25
	80	0.02	3.22	1041.41	3.25
	160	0.02	0.01	102.94	3.34
5	10	3.14	-	860769.22	-
	20	0.05	6.01	94620.77	3.19
	40	0.01	1.72	9931.49	3.25
	80	0.02	-0.07	1040.04	3.26
	160	0.02	-0.11	103.81	3.32
6	10	0.10	-	860765.07	-
	20	0.01	2.90	94674.15	3.18
	40	0.01	-0.07	9935.76	3.25
	80	0.02	-0.08	1036.02	3.26
	160	0.02	-0.13	102.85	3.33

Table 5.2: Convergence with respect to Δz for $\Delta t = 10^{-4}$ with generalized moment limiter and viscosity limiter using RK3ssp

p	$\frac{1}{\Delta z}$	Gen. moment limiter		Viscosity limiter	
		$10^9 \ \varepsilon\ _1$	order	$10^9 \ \varepsilon\ _1$	order
1	10	2049303.44	-	2049541.01	-
	20	522694.83	1.97	522694.98	1.97
	40	132273.11	1.98	132273.11	1.98
	80	33322.24	1.99	33322.24	1.99
	160	8366.04	1.99	8366.04	1.99
2	10	150717.27	-	150654.75	-
	20	18318.29	3.04	18318.29	3.04
	40	2265.73	3.02	2265.73	3.02
	80	281.93	3.01	281.93	3.01
	160	35.17	3.00	35.17	3.00
3	10	3846.36	-	3839.79	-
	20	245.61	3.97	245.61	3.97
	40	15.58	3.98	15.58	3.98
	80	0.98	4.00	0.98	4.00
	160	0.07	3.88	0.07	3.88
4	10	147.95	-	146.54	-
	20	4.45	5.05	4.45	5.04
	40	0.14	4.97	0.14	4.97
	80	0.02	3.22	0.02	3.22
	160	0.01	0.42	0.02	0.01
5	10	4.58	-	3.14	-
	20	0.05	6.55	0.05	6.01
	40	0.01	1.72	0.01	1.72
	80	0.01	0.08	0.02	-0.07
	160	0.01	0.30	0.02	-0.11
6	10	1.03	-	0.10	-
	20	0.01	6.21	0.01	2.90
	40	0.01	-0.08	0.01	-0.07
	80	0.01	0.06	0.02	-0.08
	160	0.01	0.30	0.02	-0.13

Table 5.3: Convergence with respect to Δt for $p = 5$ with no slope limiter, generalized moment limiter and viscosity limiter using RK3ssp, with Arprec 100 precision digits

Δt	No limiter			Gen. moment limiter			Viscosity limiter		
	$\frac{1}{\Delta z}$	$10^{12}\ \varepsilon\ _1$	order	$\frac{1}{\Delta z}$	$10^{12}\ \varepsilon\ _1$	order	$\frac{1}{\Delta z}$	$10^{12}\ \varepsilon\ _1$	order
10^{-3}	40	19316.90	-	160	37733.82	-	20	15743.84	-
10^{-4}	160	16.73	3.06	160	11.37	3.52	160	16.73	2.97
10^{-5}	160	0.01	3.05	160	0.01	2.92	160	0.01	3.05

THIS PAGE INTENTIONALLY LEFT BLANK

Chapter 6

Runge-Kutta discontinuous Galerkin method for the Boltzmann equation

The Runge-Kutta discontinuous Galerkin method (RKDG) has been successfully applied to the nondimensional collisionless Boltzmann equation for one node in velocity space for both continuous and discontinuous distribution function in chapters 4 and 5 respectively. High-order accuracy in physical space and time has been observed for both the continuous and discontinuous problem.

In this chapter, a procedure to adapt the RKDG method to the Boltzmann equation is described in detail. The physical space is discretized with the discontinuous Galerkin method. The time discretization is achieved using a strong stability-preserving (SSP) Runge-Kutta scheme to ensure stability. The collision integral $[\frac{df}{dt}]_{\text{coll}}$ is evaluated using the particle-like method developed in [4].

6.1 Discretization of velocity space

The distribution function is defined over a velocity space that extends from $-\infty$ to ∞ in all three dimensions. However, in the interest of computational efficiency, only a finite number of discrete values of \vec{v} are considered in the range $-4 < v_x, v_y, v_z < 4$.

This truncation is justified in low speed flows where the distribution function is known to decay to zero very fast with increasing $|\vec{v}|$. Each velocity dimension is discretized into n_v nodes, giving a total of n_v^3 nodes in the three-dimensional truncated velocity space.

6.2 Discontinuous Galerkin discretization

The nondimensional collisionless Boltzmann equation is discretized in the physical space by the discontinuous Galerkin method as given in section 3.1. The same physical space elements, modal basis functions of Legendre polynomials and initialization of distribution function are used. The nondimensional Boltzmann equation discretized in the physical space by the discontinuous Galerkin method in terms of modal coefficients is also similar, with an addition of the collision integral term,

$$\begin{aligned} \frac{\partial \tilde{f}_j^l}{\partial t} &= \frac{\sqrt{\pi}}{2} v_z \frac{2l+1}{\Delta z} \left[\sum_m 2\tilde{f}_j^m + \sum_{k=0}^p \left((-1)^l h(\tilde{f}_{j-1}^k, (-1)^k \tilde{f}_j^k) - h(\tilde{f}_j^k, (-1)^k \tilde{f}_{j+1}^k) \right) \right] \\ &+ \left[\frac{d\tilde{f}_j^l}{dt} \right]_{\text{coll}} \end{aligned} \quad (6.1)$$

where $\left[\frac{d\tilde{f}_j^l}{dt} \right]_{\text{coll}}$ is the collision integral expressed in terms of modal coefficients.

As in the case of equation (3.24) for the collisionless case, equation (6.1) can be expressed as

$$\begin{aligned} \frac{\partial \tilde{f}_j}{\partial t} &= \tilde{L}_j(\tilde{f}_j) + \left[\frac{d\tilde{f}_j}{dt} \right]_{\text{coll}} \\ &= \left[\frac{\partial \tilde{f}_j}{\partial t} \right]_{\text{colless}} + \left[\frac{d\tilde{f}_j}{dt} \right]_{\text{coll}} \end{aligned} \quad (6.2)$$

where $\left[\frac{\partial \tilde{f}_j}{\partial t} \right]_{\text{colless}} = \tilde{L}_j(\tilde{f}_j)$ is the time derivative of the modal coefficients of all orders $l \leq p$ for each element I_j for the nondimensional collisionless Boltzmann equation. This time derivative $\left[\frac{\partial \tilde{f}_j}{\partial t} \right]_{\text{colless}}$ shall be called simply the collisionless time derivative of modal coefficients. The method to solve the collisionless time derivative of modal

coefficients has been given in detail in chapter 3.

6.3 Collision integral

The collision integral is computed by the particle-like method developed in [4]. It results in significantly lower statistical uncertainty compared to DSMC. Despite this, some statistical uncertainty is present and controlled by \mathcal{N} , the number of simulated collisions per cell in velocity space. Throughout this thesis, we will set \mathcal{N} to the smallest value which results in essentially negligible statistical uncertainty.

The above particle-like method computes the collision integral for all nodes in velocity space and one node in physical space in one run. It takes in the discrete distribution function f_h at one node z_i in physical space over all nodes in the truncated velocity space \vec{v} , and generates the collision integral $\left[\frac{df_h}{dt}\right]_{\text{coll}}$ for the discrete distribution function at the same node z_i for all \vec{v} . This means that to compute the collision integral for all the n_z nodes in the physical space and n_v^3 nodes in the truncated velocity space, the routine for computing collision integral has to be called n_z times (once for each node in physical space). More about the value of n_z and the positions of the nodes z_i to be taken for the discrete distribution function are discussed in the next section.

Note that this method of computing collision integral takes in discrete distribution function f_h and not the modal coefficients \tilde{f} as input. Therefore, the collision integral cannot be expressed in terms of modal coefficients as discussed in section 6.2.

6.4 Runge-Kutta time discretization

The nondimensional Boltzmann equation has been discretized in physical space by the discontinuous Galerkin method and expressed as a function of modal coefficients in equation (6.2). However, as stated above, we cannot compute the collision integral for distribution functions in terms of modal coefficients.

In order to use the method in section 6.3 to compute the collision integral, equation

(6.2) should be converted to be in terms of the discrete distribution function f_h evaluated at $p + 1$ Gauss points in each element. The Gauss points in each element are the positions of the nodes z_i , which can be related to the Gauss points ξ_g with linear transformation of equation (3.2). The total number of nodes in the physical space is

$$n_z = n(p + 1) \quad (6.3)$$

where n is the total number of elements I_j in the physical space.

The collisionless time derivative of modal coefficients, $\left[\frac{\partial \tilde{f}_j}{\partial t}\right]_{\text{colless}}$, should be expressed as a time derivative of the discrete distribution function evaluated at the n_z nodes. Putting the collisionless time derivative of modal coefficients into equation (3.9), the following equation is derived

$$\left[\frac{\partial f_h(\xi)}{\partial t}\right]_{\text{colless}} = \sum_{k=0}^p \psi^k(\xi) \left[\frac{\partial \tilde{f}_j^k}{\partial t}\right]_{\text{colless}} \quad (6.4)$$

This collisionless time derivative can be mapped from dimension ξ to z with equation (3.2). The collisionless time derivative $\left[\frac{\partial f_h(z)}{\partial t}\right]_{\text{colless}}$ has to be computed for all n_z nodes in the physical space z and for all n_v^3 nodes in the truncated velocity space \vec{v} .

Before updating the discrete distribution function, the collision integral $\left[\frac{df_h(z)}{dt}\right]_{\text{coll}}$ for all n_z nodes in the physical space and n_v^3 nodes in the truncated velocity space has to be computed by the particle-like method n_z times.

The discrete distribution function f_h can then be updated with the following time derivative, for all nodes in physical space and truncated velocity space,

$$\frac{\partial f_h}{\partial t} = \left[\frac{\partial f_h}{\partial t}\right]_{\text{colless}} + \left[\frac{df_h}{dt}\right]_{\text{coll}} \quad (6.5)$$

The RK3ssp scheme has been proven to be stable and third-order accurate in time. The RK3ssp method shall be used for time discretization in this chapter. The algorithm of the RK3ssp method for advancing one time step Δt_k from t_k to t_{k+1} is given in equation (3.31).

6.5 Slope limiter

Discontinuities are present in the distribution function for each node in the truncated velocity space. For the test problem of chapter 5, despite the presence of oscillations around the discontinuities, the results in section 5.6 have shown that slope limiters are not necessary to ensure stability provided the time steps are small enough to satisfy the Courant-Friedrichs-Levy (CFL) condition given in equation (3.29).

However, the presence of oscillations also means that the solution is not accurate near the discontinuities. Section 5.6 has shown that the viscosity limiter is the most effective in limiting the oscillations while maintaining high-order accuracy in physical space and time for the smooth regions away from the discontinuities. Therefore, in this chapter, we shall compare the solutions with and without the viscosity limiter.

The viscosity limiter is applied as described in section 3.3.2. The viscosity parameter is set to $\nu_0 = 0.1$.

6.6 Implementation

The RKDG method for the nondimensional Boltzmann equation has been implemented in C++. The high computational cost of evaluating the distribution function for all n_z nodes in the physical space z and for all n_v^3 nodes in the truncated velocity space prohibits efficient implementation in Matlab.

The following is the RKDG algorithm for the nondimensional Boltzmann equation for one physical dimension z and three dimensions in the truncated velocity space:

1. Initialize by evaluating the discrete distribution function f_h at all the n_z Gauss points in the physical space with equations (2.11), (2.12) and (3.12). Repeat the initialization of the discrete distribution function for each of the n_v^3 nodes in the truncated velocity space $-4 < v_x, v_y, v_z < 4$.
2. Generate the matrices \mathbf{L}^+ and \mathbf{L}^- according to equations (3.20) and (3.26). Note that the same matrices can be used for all nodes in the truncated velocity space.

3. Compute the collision integral $\left[\frac{df_h(z)}{dt}\right]_{\text{coll}}$ for all the n_z Gauss points in the physical space using the particle-like method n_z times. Do not update the distribution function.
4. Convert the distribution function at the n_z Gauss points to modal coefficients \tilde{f}_j^l for all orders $l = 0$ to p in every element I_j from equation (3.11) for each of the n_v^3 nodes.
5. Evaluate the collisionless time derivative of the modal coefficients $\left[\frac{\partial \tilde{f}_j}{\partial t}\right]_{\text{colless}} = \tilde{L}_j(\tilde{f}_i)$ for every element I_j with equation (3.26) for each of the n_v^3 nodes in the velocity space \vec{v} . If desired, limit the change in modal coefficients due to the collisionless time derivative with the viscosity limiter.
6. Convert the collisionless time derivative to be in terms of discrete distribution functions $\left[\frac{\partial f_h(z)}{\partial t}\right]_{\text{colless}}$ at the n_z Gauss points with equations (6.4) and (3.2) for each of the n_v^3 nodes.
7. Compute the time derivative $\frac{\partial f_h}{\partial t}$ with equation (6.5).
8. Update the intermediate discrete distribution function $f_h^{(i)}$ for one intermediate stage of RK3ssp according to equation (3.31).
9. Repeat steps 3 to 8 for each intermediate Runge-Kutta stage till one RK3ssp time step is completed. Update the discrete distribution function with the intermediate discrete distribution functions $f_h^{(i)}$ according to equation (3.31).
10. Repeat step 9 for each time step.

6.7 Comparison with direct simulation Monte Carlo (DSMC)

The Couette flow problem described in section 2.2 for Knudsen numbers $\text{Kn} = 0.1, 1$ and 10 are to be solved using the RKDG method for the nondimensional Boltzmann

equation. The number of elements and the order of approximation in the physical space are set to $n = 10$ and $p = 2$ respectively, and integrated in time from $t = 0$ using RK3ssp. The mean velocity u_x and shear stress p_{xz} shall be calculated with equations (2.13) and (2.14) respectively at the various time instants shown in table 6.1.

The mean velocity and shear stress at the same time instants are also obtained by averaging 60 ensembles of the direct simulation Monte Carlo (DSMC) method using 100 elements in physical space and 2×10^5 particles per element. The results from the DSMC method are compared with those from the RKDG method.

We first test the RKDG solution method without slope limiters. The number of nodes used in the truncated velocity space are $n_v^3 = 30^3$ and 50^3 . The test parameters for each characteristic flow length scale, $\text{Kn} = 0.1, 1$ and 10 , are described in table 6.1, and the resulting mean velocity and shear stress are shown in figures 6-1, 6-2 and 6-3. Note that for $\text{Kn} = 0.1$ with $n_v^3 = 30^3$, a value of $\mathcal{N} = 0.1$ results in observable statistical uncertainty; for this reason, \mathcal{N} is set to 1.0 for this calculation.

The mean velocity and shear stress profiles agree well with DSMC results, but oscillations are present in some cases. For the coarse velocity space discretization of $n_v^3 = 30^3$, oscillations are present in the shear stress for $\text{Kn} = 1$ and 10 . Oscillations can also be seen in the mean velocity for $\text{Kn} = 10$ with $n_v^3 = 30^3$. Moreover, a small discrepancy in the steady state shear stress can be observed for $\text{Kn} = 0.1$ with $n_v^3 = 30^3$.

With a finer velocity space discretization of $n_v^3 = 50^3$, the steady state shear stress of the RKDG method for $\text{Kn} = 0.1$ is closer to that of DSMC. Furthermore, the oscillations have been effectively removed for all cases. However, using more nodes in the velocity space greatly increases the computational cost. The computational cost with $n_v^3 = 50^3$ is about $(\frac{5}{3})^3 \approx 4.63$ times of that with $n_v^3 = 30^3$. We seek more efficient ways of eliminating the oscillations.

6.7.1 Viscosity limiter

When the characteristic flow length scale is relatively small ($Kn = 1$ and 10), oscillations around discontinuities in the distribution function contribute to most of the oscillations in the RKDG solutions. These oscillations can be removed by applying the viscosity limiter as we show in figure 6-4. The test parameters with the viscosity limiter are listed in table 6.2.

The viscosity limiter has effectively removed the oscillations in both the mean velocity and shear stress profiles. However, the transient shear stress evaluated by RKDG are slightly more negative than the shear stress evaluated by DSMC, while the steady state solutions of RKDG are very close to the DSMC solutions. Compared to the computationally expensive way of making the velocity space discretization finer, the viscosity limiter is much more efficient and provides good steady state solutions, but it has the trade-off of giving slightly more negative transient shear stress.

Table 6.1: Test parameters for $\text{Kn} = 0.1, 1$ and 10

Kn	n_v^3	\mathcal{N}	Δt	Time instants				
				t_0	t_1	t_2	t_3	t_4
0.1	30^3	1.0	0.002	0	2.04	4.96	11.96	32.04
	50^3	0.1						
1	30^3 or 50^3	0.1	0.0002	0	0.204	0.496	1.016	4.016
10	30^3 or 50^3	0.1	0.00002	0	0.0204	0.0496	0.1602	0.5640

Table 6.2: Test parameters for $\text{Kn} = 1$ and 10 with viscosity limiter

Kn	n_v^3	\mathcal{N}	ν_0	Δt	Time instants				
					t_0	t_1	t_2	t_3	t_4
1	30^3	0.1	0.1	0.0002	0	0.204	0.496	1.016	4.016
10	30^3	0.1	0.1	0.00002	0	0.0204	0.0496	0.1602	0.5640

(a) $n_v^3 = 30^3$

(b) $n_v^3 = 50^3$

Figure 6-1: Mean velocity and shear stress in Couette flow for $\text{Kn} = 0.1$ and $u_{\text{wall}} = \pm 0.1$ at $t = 0, 2.04, 4.96, 11.96$ and 30.02 . Comparison of RKDG with $n = 10$ and $p = 2$ against DSMC

(a) $n_v^3 = 30^3$

(b) $n_v^3 = 50^3$

Figure 6-2: Mean velocity and shear stress in Couette flow for $\text{Kn} = 1$ and $u_{\text{wall}} = \pm 0.1$ at $t = 0, 0.204, 0.496, 1.016$ and 4.016 . Comparison of RKDG with $n = 10$ and $p = 2$ against DSMC

(a) $n_v^3 = 30^3$

(b) $n_v^3 = 50^3$

Figure 6-3: Mean velocity and shear stress in Couette flow for $\text{Kn} = 10$ and $u_{\text{wall}} = \pm 0.1$ at $t = 0, 0.0204, 0.0496, 0.1602$ and 0.5640 . Comparison of RKDG with $n = 10$ and $p = 2$ against DSMC

(a) $\text{Kn} = 1$ at $t = 0, 0.204, 0.496, 1.016$ and 4.016

(b) $\text{Kn} = 10$ at $t = 0, 0.0204, 0.0496, 0.1602$ and 0.5640

Figure 6-4: Mean velocity and shear stress in Couette flow for $\text{Kn} = 1$ and 10 and $u_{\text{wall}} = \pm 0.1$. Comparison of RKDG with $n = 10, p = 2$ and viscosity limiter against DSMC

THIS PAGE INTENTIONALLY LEFT BLANK

Chapter 7

Conclusion

Using analytical solutions of simple continuous and discontinuous problems, the high-order convergence of the RKDG method has been verified. For the test problem with discontinuous solutions, the RKDG method is stable even without the use of slope limiters; additionally, in the presence of discontinuities, it exhibits high-order accuracy in both physical space and time (away from the discontinuities). With a viscosity limiter, the oscillations are eliminated while the high-order accuracy is retained.

For the Boltzmann equation, an RKDG solution method has been developed by formulating the collision integral as a source term to the advection equation. For the Couette flow problem of characteristic flow length scales of $\text{Kn} = 0.1, 1$ and 10 , the mean velocity and shear stress computed by the RKDG method are close to those obtained with DSMC. A finer velocity space discretization of $n_v^3 = 50^3$ gives very good results, while with a coarser discretization of $n_v^3 = 30^3$, oscillations are observed in the mean velocity and especially in the shear stress for $\text{Kn} \gtrsim 1$. The viscosity limiter is effective in removing these oscillations.

The RKDG solution method developed in this thesis has shown good agreement with DSMC results even with a coarse physical space discretization, proving that this is a viable direct numerical method for the Boltzmann equation.

7.1 Future work

7.1.1 High-order physical space discretization

The high-order accuracy in physical space of RKDG has been verified with the test problems with nondimensional collisionless Boltzmann equation in chapters 4 and 5. Higher-order physical space discretization has not been used for the nondimensional Boltzmann equation in chapter 6 because of the good results that are already obtained with a coarse physical space discretization.

The viscosity limiter has been shown to work well for high-order physical space discretization ($p > 2$) in the test problem with discontinuous solution of chapter 5. Theoretically, with the appropriate viscosity, the viscosity limiter should continue to be effective in eliminating oscillations for higher-order physical space discretization for the nondimensional Boltzmann equation. More tests can be done for the RKDG solution method with higher-order physical space discretization.

7.1.2 Viscosity in the viscosity limiter

Equation (3.41) for the computation of viscosity ν is a simplified form. A more computationally intensive form that gives a smooth viscosity profile is described in [16], but for our Boltzmann equation problems, it does not give significantly different results compared to the simplified form used here. Another method of computing viscosity, by relating the viscosity to the real physical dissipation for an ideal gas problem, has also been developed in [16, 15]. Further work can be carried out to relate the viscosity to the Boltzmann equation.

7.1.3 High-order velocity space discretization

Currently, the velocity space is discretized with an effective order of $p = 0$, which means that the method is only accurate to $O(n_v)$, where n_v is the number of nodes in one dimension of the truncated velocity space. The importance of velocity space discretization is highlighted by the results in section 6.7, where the oscillations in the

mean velocity and shear stress are very much reduced by using more nodes in the truncated velocity space. The velocity space can be discretized with some interpolation methods, for example the Galerkin method, to give higher-order accuracy in the velocity space. Having higher-order accuracy in the velocity space can lead to similar accuracy using less nodes in the velocity space, leading to lower computational cost.

THIS PAGE INTENTIONALLY LEFT BLANK

Appendix A

Gaussian quadrature

Gaussian quadrature, also known as Gauss-Legendre quadrature, is a commonly used numerical integration technique for integrals over a finite interval. In this thesis, integration is always done over the reference element of $\xi \in [-1, 1]$. This means that the integral can be evaluated numerically using Gaussian quadrature without variable transformation

$$\int_{-1}^1 f(\xi) d\xi \approx \sum_{n_g} w_g f(\xi_g) \quad (\text{A.1})$$

where n_g is the number of Gauss points used, ξ_g are the Gauss points, and w_g are the corresponding Gauss weights. The number of Gauss points to be used depends on the accuracy desired. The Gaussian quadrature with n_g Gauss points is able to integrate a polynomial up to order $k = 2n_g - 1$ exactly.

Table A.1 shows the Gauss points and weights for up to $n_g = 7$. Gauss points and weight for larger n_g can be found in [5].

Table A.1: Gauss points and weights for $n_g \leq 7$

n_g	k	ξ_g	w_g
2	3	$\pm \frac{\sqrt{3}}{3} \approx \pm 0.577350$	1
3	5	0 $\pm \frac{\sqrt{15}}{5} \approx \pm 0.774597$	$\frac{8}{9} \approx 0.888889$ $\frac{5}{9} \approx 0.555556$
4	7	$\pm \frac{1}{35} \sqrt{525 - 70\sqrt{30}} \approx \pm 0.339981$ $\pm \frac{1}{35} \sqrt{525 + 70\sqrt{30}} \approx \pm 0.861136$	$\frac{1}{36} (18 + \sqrt{30}) \approx 0.652145$ $\frac{1}{36} (18 - \sqrt{30}) \approx 0.347855$
5	9	0 $\pm \frac{1}{21} \sqrt{245 - 14\sqrt{70}} \approx \pm 0.538469$ $\pm \frac{1}{21} \sqrt{245 + 14\sqrt{70}} \approx \pm 0.906180$	$\frac{128}{225} \approx 0.568889$ $\frac{1}{900} (322 + 13\sqrt{70}) \approx 0.468729$ $\frac{1}{900} (322 - 13\sqrt{70}) \approx 0.236927$
6	11	± 0.238619 ± 0.661209 ± 0.932470	0.467914 0.360762 0.171324
7	13	0 ± 0.405845 ± 0.741531 ± 0.949108	0.417959 0.381830 0.279705 0.129485

Bibliography

- [1] V. V. Aristov. *Direct Methods for Solving the Boltzmann Equation and Study of Nonequilibrium Flows*. Kluwer Academic Publishers, Dordrecht, Netherlands, 2001.
- [2] D. H. Bailey, Y. Hida, K. Jeyabalan, X. S. Li, and B. Thompson. Arbitrary precision computation package (ARPREC). World Wide Web, <http://crd.1bl.gov/~dhbailey/mpdist/>, June 2006.
- [3] L. Baker. Efficient numerical methods for solving the Boltzmann equation for low-speed flows. Master's thesis, Massachusetts Institute of Technology, February 2004.
- [4] L. L. Baker and N. G. Hadjiconstantinou. Variance reduction for Monte Carlo solutions of the Boltzmann equation. *Physics of Fluids*, 17(051703), 2005.
- [5] W. H. Beyer. *CRC Handbook of Mathematical Sciences*. CRC Press, West Palm Beach, Florida, 6th edition, 1987.
- [6] G. A. Bird. *Molecular Gas Dynamics and the Direct Simulation of Gas Flows*. Clarendon Press, Oxford, 1994.
- [7] R. Biswas, K. D. Devine, and J. E. Flaherty. Parallel, adaptive finite element methods for conservation laws. *Applied Numerical Mathematics*, 14:255–283, 1994.

- [8] J. C. Butcher. *The Numerical Analysis of Ordinary Differential Equations: Runge-Kutta and General Linear Methods*. John Wiley & Sons, Chichester, 1987.
- [9] B. Cockburn and C.-W. Shu. The local discontinuous Galerkin method for time-dependent convection-diffusion systems. *SIAM Journal on Numerical Analysis*, 35(6):2440–2463, 1998.
- [10] B. Cockburn and C.-W. Shu. Runge-Kutta discontinuous Galerkin methods for convection-dominated problems. *Journal of Scientific Computing*, 16(3):174–261, September 2001.
- [11] S. Gottlieb, C.-W. Shu, and E. Tadmor. Strong stability-preserving high-order time discretization methods. *SIAM Review*, 43(1):89–112, 2001.
- [12] The MathWorks Inc. MATLAB programming: Floating-point numbers. World Wide Web, http://www.mathworks.com/access/helpdesk/help/techdoc/matlab_prog/f2-98645.html, 2006.
- [13] G. E. Karniadakis and S. J. Sherwin. *Spectral/hp Element Methods for Computational Fluid Dynamics*. Oxford University Press, New York, 2nd edition, 2005.
- [14] J. Von Neumann and R. D. Richtmyer. A method for the numerical calculation of hydrodynamic shocks. *Journal of Applied Physics*, 21, 1950.
- [15] V. T. Nguyen, B. C. Khoo, J. Peraire, and P.-O. Persson. Shock capturing scheme in high order discontinuous Galerkin method. In *7th WCCM*, Los Angeles, CA, July 2006.
- [16] P.-O. Persson and J. Peraire. Sub-cell shock capturing for discontinuous Galerkin methods. In *AIAA-2006-0112, 44th Aerospace Sciences Meeting*, Reno, NV, 2006.

- [17] W. H. Press, B. P. Flannery, S. A. Teukolsky, and W. T. Vetterling. *Numerical Recipes in C : The Art of Scientific Computing*. Cambridge University Press, Cambridge, 2nd edition, 1992.
- [18] F. Reif. *Fundamentals of Statistical and Thermal Physics*. McGraw-Hill, Boston, 1965.
- [19] C.-W. Shu. TVB uniformly high-order schemes for conservation laws. *Mathematics of Computation*, 49(179):105–121, July 1987.
- [20] W. G. Vincenti and C. H. Kruger. *Introduction to Physical Gas Dynamics*. Krieger, Florida, 1965.